Research Square

Preprints are preliminary reports that have not undergone peer review.
They should not be considered conclusive, used to inform clinical practice,
or referenced by the media as validated information.

Adenyl cyclase 6 is an evolutionary conserved chief regulator of peripheral nerve development and timely myelination in vertebrates

Océane El-Hage
INSERM U1195: Maladies et hormones du systeme nerveux
Marie-José Boueid
INSERM U1195: Maladies et hormones du systeme nerveux
Fanny Magné
Fondation Ophtalmologique Adolphe de Rothschild: La Fondation Adolphe de Rothschild
Andoni Echaniz-Laguna
CHU Bicêtre: Hopital Bicetre
Judith Melki
INSERM U1195: Maladies et hormones du systeme nerveux
Marcel Tawk
marcel.tawk@inserm.fr

INSERM https://orcid.org/0000-0003-4267-4743

Research Article

Keywords: Adcy6, Schwann cell, zebrafish, mice, cAMP, peripheral nervous system, myelin, Gpr126, Adcy5, AMC

Posted Date: June 30th, 2026

DOI: https://doi.org/10.21203/rs.3.rs-10087866/v1

License: This work is licensed under a Creative Commons Attribution 4.0 International License.
Read Full License

Version of Record: A version of this preprint was published at Cellular and Molecular Life Sciences on October 2nd, 2026. See the published version at https://doi.org/10.1007/s00018-026-06443-3.

Adenyl cyclase 6 is an evolutionary conserved chief regulator of peripheral nerve development and timely myelination in vertebrates

Océane El-Hage[1#*], Marie-José Boueid[1#], Fanny Magné[1,2], Andoni Echaniz-Laguna[1,3,4], Judith Melki[1], Marcel Tawk[1*]

[1] Université Paris-Saclay, INSERM, Neuro-Bicêtre U1195, 94276 Le Kremlin-Bicêtre, France
[2]Fondation ophtalmologique Adolphe de Rotschild, Neurology Department, Paris, France
[3]Neurology Department, APHP, CHU de Bicêtre, Le Kremlin-Bicêtre, 94276, France
[4] French National Reference Centre for Rare Neuropathies (CERAMIC), Le Kremlin-Bicêtre, 94276, France
[#] These authors contributed equally to this work
[*]correspondence to: oceane.el-hage@inserm.fr; marcel.tawk@inserm.fr

Key words: Adcy6, Schwann cell, zebrafish, mice, cAMP, peripheral nervous system, myelin, Gpr126, Adcy5, AMC

Abstract

Myelination of large caliber axons by Schwann cells and clustering of ion channels at the nodes of Ranvier enables electrical impulses to propagate rapidly along axons in the peripheral nervous system (PNS). Although several *in vitro* studies have reported a role for the cyclic adenosine monophosphate (cAMP) in regulating the proliferation and differentiation of Schwann cells, the identity of the *in vivo* key regulator of cAMP and its broad role in peripheral nerve development remains unknown. Drawing on pharmacological, genetic, molecular, and live-imaging experiments in zebrafish and mice, we find that adenyl cyclase 6, *Adcy6*, albeit in synergy with *Adcy5* in mice, is required within Schwann cells for timely radial sorting and myelination in the PNS, without affecting the distribution and proliferation of Schwann cells along peripheral nerves. Our analysis also shows that Adcy6 is the main driver of early Gpr126 signaling, required for timely myelin gene expression, upstream of PKA. In addition, we show that *Adcy6*$^{-/-}$ *Adcy5*$^{-/-}$ mice present excess mortality, severe tremor, reduced nerve size, defective nerve conduction and motor dysfunction, highlighting both axonal and glial defects. We provide evidence that Adcy6 regulates neuronal numbers, mediates axonal transport and impacts, autonomously in neurons, upon sodium channel clustering. Together, our findings

identify Adcy6 as a primary driver of early and timely cAMP activity, *in vivo,* during the development of the PNS in vertebrates.

Introduction

Schwann cells (SCs) wrap axons with a myelin sheath in the peripheral nervous system (PNS) [1–3]. Myelin is an evolutionary feature of vertebrates, allowing SCs to synthesize great amounts of membrane to ensure peripheral myelin sheath growth around large caliber axons[4]. This, in turn, promotes fast nerve conduction velocity without the necessity to dramatically increase axonal diameter[5,6]. The proliferation and differentiation of SCs depend on the ubiquitous second messenger cyclic adenosine monophosphate (cAMP); the relevance of which in myelinating SCs *in vitro*, has been documented as early as the 1980s[7–11]. Several molecules have been identified to modulate cAMP signaling during developmental peripheral myelin formation. For instance, the adhesion G protein coupled receptor Gpr126 is shown to directly increase cAMP by coupling to heterotrimeric G-proteins [12–14]. Despite its importance, the identity of the key molecule which is responsible for the synthesis of cAMP *per se* within the PNS remains unknown.

We have previously shown that a homozygous missense mutation in the adenyl cyclase 6, *ADCY6 (AC6),* was responsible for severe arthrogryposis multiplex congenita (AMC), characterized by congenital contractures and, importantly, a lack of peripheral myelin in the PNS[15]. *ADCY6* belongs to a membrane-bound family of enzymes that utilize adenosine triphosphate (ATP) to generate cAMP, and thereby relays membrane signaling to second messenger[16]. Moreover, a mutation in *GPR126* has been linked to AMC that coincides with defective peripheral myelination[17]. Gpr126 has emerged as a chief SC component required for peripheral myelin formation in vertebrates, linking signaling from the extracellular matrix to cAMP[18]. Thus, mutations in *ADCY6* and *GPR126* would alter cAMP activity, disrupt mechanisms of myelin formation in humans and contribute to severe congenital diseases such as AMC.

Adenyl cyclases stand as strong candidate mediators of cAMP activity in peripheral myelination; however, the identity and the potential role of adenyl cyclases in mediating cAMP-regulated peripheral myelination *in vivo,* have not yet been investigated. Moreover, we do not know whether adenyl cyclases' activity would affect different stages of SC developmental progression or would regulate neuronal/axonal development in the PNS *in vivo*. Understanding the role of adenyl cyclases in peripheral nerve development would open up new

therapeutic opportunities, given that targeting canonical GPCR/G-protein-cAMP signaling pathway account for an important share of marketed drugs against a wide range of diseases[19]. As such, Adcy6 is an ideal candidate and is likely to be one of the missing adenyl cyclases that links Gpr126 to cAMP and drives SC timely myelination *in vivo*.

Here, we investigate the role of Adcy6 signaling in peripheral nerve development *in vivo* using two vertebrate animal models: zebrafish and mice. We provide evidence that Adcy6 is a primary adenyl cyclase which mediates early myelin sheath growth in the PNS of vertebrates, and drives myelin gene expression, mainly via the Gpr126-cAMP-PKA pathway. Moreover, we show that Adcy6 is required for neuronal development, axonal transport and the clustering of voltage-gated sodium channels. This study reveals, for the first time, the identity and specificity of the adenyl cyclase that initiates early and timely cAMP activity in the developing PNS of vertebrates, shedding light into its role in human fetal development.

Results

Adcy6 mice are viable but show late onset of peripheral axonal wrapping

We first evaluated Adcy6 expression in the mice sciatic nerve and dorsal root ganglia (DRG). Adcy6 was detectable in the wild-type (WT) mice sciatic nerves at postnatal day 5 (P5) and maintained its expression to adulthood (Figure 1A and Figure S1). Adcy6 expression was also detected in DRG derived from mice embryos at E13 (Figure 1A). Moreover, analysis of published expression datasets revealed that Adcy6 is expressed in SC[20]. To understand the role of Adcy6 in PNS development, we first analyzed *Adcy6* knockout (KO) mice[21,22]. *Adcy6*$^{-/-}$ animals were born in expected Mendelian ratios and survived to adulthood. We therefore examined sciatic nerve ultrastructure using transmitted electron microscopy (TEM) at several developmental stages in *Adcy6*$^{-/-}$ and control mice. The ultrastructure analysis revealed a significant reduction in the number of myelinated axons at P5 in *Adcy6*$^{-/-}$ mice mutant sciatic nerves in comparison to controls (Figure 1B,C). Similar defects were observed at P10, however, the number of myelinated axons in *Adcy6*$^{-/-}$ sciatic nerves was comparable to controls at adulthood (Figure 1B,C). We did not observe a significant difference in the total number of axons per field between control and mutant sciatic nerves at all examined stages (Figure 1D). We also found that SCs were temporarily blocked at the pro-myelin stage at P5, since a significant proportion of large diameter axons engaged in a 1:1 relationship was devoid of myelin sheet (Figure 1E-H). When myelin sheet was present, the G-ratio was comparable between all groups at all examined stages (Figure 1I). These observations were in line with

RT-qPCR analyses of extracted mRNAs, showing a significant decrease in the expression of several SC myelin markers at P5 such as *Mbp, Pmp22* and *Mpz* in sciatic nerves (Figure 1J-L). In contrast, the expression of the earlier SC marker, *Sox10* was not altered at all stages, indicating that SCs are present along the mutant nerves (Figure 1J-L). This result demonstrates that the absence of Adcy6 leads to a significant delay in myelin development.

To investigate the function of Adcy6 specifically in SC, we crossed $Adcy6^{lox/lox}$ mice with mice carrying Cre recombinase under the control of *Mpz* promoter. Unlike constitutive $Adcy6^{-/-}$ mutants, which showed a significant decrease in the number of myelinated axons at P5, we did not observe any delay in the development of myelinated axons in the sciatic nerves of $Adcy6^{lox/lox}$ MPZ^{cre+} mice at P5 and adulthood (Figure 1M,N). Moreover, analysis of G-ratio showed no significant difference in myelin thickness between mutants and control mice (Figure 1O). These results suggest that Adcy6 could function redundantly with another adenyl cyclase in SC in mice and/or exert its function in neurons to impact upon peripheral myelination. It is important to note that these two hypotheses are not mutually exclusive.

Adcy6 and Adcy5 present synergistic interactions and multiple abnormalities are observed in $Adcy5^{-/-}$ $Adcy6^{-/-}$ peripheral nerves

To explore a possible functional redundancy between Adcy6 and another adenyl cyclase in PNS development in mice, we decided to analyze *Adcy5* KO mice, $Adcy5^{-/-}$ [22,23]. Adcy5 and Adcy6 share ~65% amino acid sequence homology and are both activated by stimulatory G protein (Gs)[24,25]. Similar to Adcy6 expression, although significantly lower, we detected Adcy5 mRNA in the WT sciatic nerves at P5 as well as in DRG derived from mice embryos at E13 (Figure 2A). Adcy5 expression was maintained in sciatic nerve at adulthood (Figure S1). Analysis of published expression database showed that Adcy5 is also expressed in SC[20]. $Adcy5^{-/-}$ mice were born at the expected Mendelian ratio, were indistinguishable from littermates and lived to adulthood with no visible gross abnormalities. However, the double $Adcy5^{-/-}$ $Adcy6^{-/-}$ mutant pups developed significant tremor, uncoordinated movement and limb posture abnormalities that were readily observable by P5 (Figure 2B and Movie S1). They remained fragile and smaller in size until at least P23 of age, with a significant increase in mortality (Figure 2B,C). Moreover, $Adcy5^{-/-}$ $Adcy6^{-/-}$ adult mice showed abnormal hindlimb clasping upon tail suspension (Figure 2D-F and Movie S2) and a significant impairment of motor performance following pole test, presenting particular difficulties in using their hindlimbs to cling to the pole (Figure 2G,H and Movie S3). Electrophysiological analysis revealed abnormal motor nerve conduction in $Adcy5^{-/-}$ $Adcy6^{-/-}$ mice, including a major increase in the latency and

duration of the compound muscle action potential (CMAP), as well as a 50% decrease in CMAP amplitude (Figure 2I,J and Figure S2A).

We next examined nerve morphology on cross-sections of mouse sciatic nerves by light microscopy as well as TEM. First, we observed that the sciatic nerves of *Adcy5*$^{-/-}$ *Adcy6*$^{-/-}$ mice were thinner and more translucent than those of controls (Figure 3A). In P5 control and *Adcy5*$^{-/-}$ mice, many SC have already wrapped axons with myelin (Figure 3B,C). In contrast, myelin formation was significantly delayed in *Adcy6*$^{-/-}$, while the number of radially sorted axons was significantly reduced and no myelin was observed in *Adcy5*$^{-/-}$ *Adcy6*$^{-/-}$ mice (Figure 3B-D). The significant reduction in the number of myelinated axons was also observed at P10 in *Adcy5*$^{-/-}$ *Adcy6*$^{-/-}$ and *Adcy6*$^{-/-}$ mice, but only in *Adcy5*$^{-/-}$ *Adcy6*$^{-/-}$ mice in adulthood when analyzed in the whole nerve (Figure 3M). Moreover, our analysis showed that when SCs were engaged in 1:1 relationship with large caliber axons, a significant proportion was blocked at the pro-myelin stage at P5 and P10 in *Adcy5*$^{-/-}$ *Adcy6*$^{-/-}$ mice (Figure 3E-H). We did not find any difference in G-ratio of myelinated axons between the different groups at all ages examined, when myelin sheath was present (Figure 3I). The total number of axons per field was globally comparable between the different groups except at P10 in *Adcy5*$^{-/-}$ *Adcy6*$^{-/-}$ mice, however the percentage of axons per diameter range showed no significant difference between the different groups (Figure 2J,K). We also found that the nerve area in *Adcy5*$^{-/-}$ *Adcy6*$^{-/-}$ mice was significantly smaller in comparison to all other groups at all stages examined (Figure 3L,N), but found no evidence for axonal degeneration. The reduction in myelinating SC was accompanied by a significant down-regulation of structural myelin markers such as *Mpz, Pmp22* and *Mbp* at P5 in *Adcy6*$^{-/-}$ mice, while structural myelin markers and the transcription factor *Krox20* were significantly down-regulated at P5 and P10 in *Adcy5*$^{-/-}$*Adcy6*$^{-/-}$ mice (Figure 3O,P). Surprisingly, the expression of *Oct6* was significantly increased in the sciatic nerves of adult *Adcy5*$^{-/-}$ *Adcy6*$^{-/-}$ mice, while *Mpz, Pmp22*, *Mbp* and *Krox20* were comparable to controls (Figure 3Q). These results show that *Adcy6* and *Adcy5* present functional synergistic interaction, required not only for timely SC myelination but also for peripheral nerve development.

Adcy6 and Adcy5 present functional synergistic interaction within Schwann cells for timely peripheral myelination

Results so far revealed an important role for Adcy6, in synergy with Adcy5, in peripheral nerve development in mice. To explore whether their functional synergistic interaction is required within SC for timely peripheral myelination, we crossed *Adcy6*$^{lox/lox}$ *MPZ*$^{cre+}$ mice with *Adcy5*$^{-/-}$

$^{-/-}$ mice. qPCR analysis confirmed efficient Cre-mediated recombination in sciatic nerves in contrast to mRNAs extracted from the brain of the same carriers (Figure S3). These mice were born at the expected Mendelian ratio, showed no gross abnormalities and were viable to adulthood. Ultrastructural analysis showed a significant decrease in the number of myelinated axons at all time points examined, as observed in *Adcy5*$^{-/-}$ *Adcy6*$^{-/-}$ mice (Figure 4A,B and O). The reduction in myelinating SC was accompanied by a significant decrease in radially sorted and sorted non-myelinated axons similar to *Adcy5*$^{-/-}$ *Adcy6*$^{-/-}$ mice (Figure 4C-G). This coincides with a down-regulation of structural myelin markers such as *Mpz, Pmp22* and *Mbp* at P5 and P10, similar to *Adcy5*$^{-/-}$ *Adcy6*$^{-/-}$ mice, while *Sox10* expression was comparable to controls at all examined stages (Figure 4H-J). Strikingly, *Adcy5*$^{-/-}$ *Adcy6*$^{lox/lox}$ *MPZ*$^{cre+}$ mutant sciatic nerves displayed a significant increase in the percentage of large caliber axons (>7µm) (Figure 4A,L), in contrast to *Adcy5*$^{-/-}$ *Adcy6*$^{-/-}$ mice. Importantly, the ratio between axonal diameter and myelin thickness was correct as revealed by G-ratios analysis, when myelin sheath was present (Figure 4M). Semi-thin cross sections analysis revealed that *Adcy5*$^{-/-}$ *Adcy6*$^{lox/lox}$ *MPZ*$^{cre+}$ mutant sciatic nerves area was comparable to controls (Figure 4N,P). Despite a reduction in the number of myelinated axons (Figure 4O), adult *Adcy5*$^{-/-}$ *Adcy6*$^{lox/lox}$ *MPZ*$^{cre+}$ mice performed well in behavioral tail suspension test and motor functional pole test and showed no difference in electrophysiological recordings, in contrast to *Adcy5*$^{-/-}$ *Adcy6*$^{-/-}$ mice (Figure 4Q-U).

These data indicate that *Adcy6* and *Adcy5* function synergistically within SC to promote timely peripheral myelination, but the delayed myelination is partially compensated for by adulthood. Moreover, a significant number of axons were able to increase their diameter, in response to the significant delay in early myelin development, perhaps due to the presence of neuronal Adcy6.

Adcy6 regulates timely myelination, but is not required for SC distribution and proliferation along peripheral nerves in zebrafish

To gain further insight into the role of Adcy6 in peripheral nerve development and myelination *in vivo* in vertebrates, we generated an *adcy6a; adcy6b* zebrafish mutant using CRISPR/Cas9 technology[26,27]. Zebrafish is a great model to study *in vivo* signaling interactions through genetic manipulation and temporal pharmacological treatment. It also allows live imaging of peripheral nerve and SC in intact embryos[28,29]. The introduced mutations engendered 10bp deletion within exon 3 of *adcy6a* and 29bp insertion in *adcy6b* within exon 3. This led to a frame shift, a premature stop codon in Adcy6a and b proteins (Figure 5A). *adcy6a*$^{-/-}$*; adcy6b*$^{-/-}$

embryos showed no obvious external defects at early stages, however, the majority of embryos (~85%) died between 3 days post fertilization (3dpf) and adulthood (Figure S4). Those who survived were significantly smaller than controls and mainly infertile, died within 6 months and developed abnormal swimming behavior (Figure 5B-E and Movie S4).

We first analyzed the ultrastructure of the posterior lateral line nerve (PLLn) using TEM. Analysis showed a dramatic decrease in the number of myelinated axons in *adcy6a*$^{-/-}$*; adcy6b*$^{-/-}$ embryos in comparison with WT. We observed an average of 0 myelinated axons per nerve in *adcy6a*$^{-/-}$*; adcy6b*$^{-/-}$ embryos at 3 dpf in comparison to 5.57 in WT (Figure 5F,G). The significant decrease in the number of myelinated axons coincided with a significant decrease in the number of radially sorted axons per nerve (Figure 5H). We also observed a significant decrease in the total number of axons in these mutants with an average of 50.64 axons in WT and 32.63 in *adcy6a*$^{-/-}$*; adcy6b*$^{-/-}$ PLLn (Figure 5I). Moreover, the percentage of myelinated axons relative to the total number of axons was significantly decreased in *adcy6a*$^{-/-}$*; adcy6b*$^{-/-}$ embryos in comparison with controls (Figure 5J). We extended this analysis to 4 and 7dpf and we observed a significant decrease in the number of myelinated axons and the total number of axons within the PLLn of mutant embryos (Figure 5F-I). Finally, the distribution of axons relative to their diameter, with a 0.1 μm bin width, showed a significant increase in the percentage of very small caliber axons (0.1-0.2 μm) in mutants compared to controls but no significant difference in the percentage of large caliber axons (Figure 5K). To determine if the myelination defect observed here is due to a reduction in SC numbers and/or proliferation, we counted the number SC and SC/PH3+ cells in *foxd3:gfp* and *adcy6a*$^{-/-}$*; adcy6b*$^{-/-}$*/foxd3:gfp* embryos. Analysis of GFP+ cells and the phospho-histone H3 antibody, which labels cells at the G2-M transition, showed no difference between WT and *adcy6a*$^{-/-}$*; adcy6b*$^{-/-}$ embryos (Figure 5L-N).

Altogether, these results show that *adcy6* is required for early radial sorting, myelination and nerve development in the PNS, as well as survival to adulthood in zebrafish.

Adcy6 is the main driver of timely Gpr126 myelin activity and mediates myelination via PKA *in vivo* in zebrafish

It has been shown that Gpr126 signaling plays an important and specific role in the initiation of peripheral myelination, and that PKA is sufficient to initiate myelination downstream of Gpr126[30]. Since GPR126 signals through cAMP to activate PKA, we hypothesize that Adcy6 may generate cAMP downstream of Gpr126 and activate PKA during early SC development. To test this hypothesis, we used an established *gpr126* morpholino (MO) that downregulates

Gpr126 function [12,31] in WT and *adcy6a*$^{-/-}$*; adcy6b*$^{-/-}$ embryos, in combination with different pharmacological compounds that impact upon cAMP and PKA activities *in vivo* (Figure 6A). We then assessed *mbp* expression along the PLLn by in situ hybridization and scored embryos into four groups based on the strength of *mbp* expression: 1-normal: comparable to WT, 2-some: reduced , 3- weak: strongly reduced and 4- no expression: undetectable (Figure 6B). *gpr126* morphants and *adcy6a*$^{-/-}$*; adcy6b*$^{-/-}$ embryos showed a significant reduction in *mbp* expression along the PLLn. Importantly, forskolin (FSK) treatment restored *mbp* expression in *gpr126* morphants, while forskolin failed to rescue *mbp* expression in *adcy6a*$^{-/-}$*; adcy6b*$^{-/-}$ and *adcy6a*$^{-/-}$*; adcy6b*$^{-/-}$*/gpr126* morphant embryos (Figure 6C). These data suggest that Adcy6 is the primary adenyl cyclase required downstream of Gp126 signaling to trigger timely myelin gene expression *in vivo*. We next treated *adcy6a*$^{-/-}$*; adcy6b*$^{-/-}$ embryos with 8-CPT-cAMP that activates cAMP-dependent PKA and Epac, and 6-Bnz-cAMP that selectively activates cAMP-dependent PKA. 8-CPT-cAMP treatment did not rescue *mbp* expression in *adcy6a*$^{-/-}$*; adcy6b*$^{-/-}$ embryos, showing a similar distribution of the phenotypic classes in comparison to DMSO *adcy6a*$^{-/-}$*; adcy6b*$^{-/-}$ treated embryos (Figure 6C). In contrast, 6-Bnz-cAMP treatment caused a significant increase in *mbp* expression in *adcy6a*$^{-/-}$*; adcy6b*$^{-/-}$ embryos, resulting in a significant shift in the distribution of the phenotypic classes in comparison to the one observed in DMSO *adcy6a*$^{-/-}$*; adcy6b*$^{-/-}$ treated embryos (Figure 6C). This result suggests that Adcy6 triggers myelin gene expression, at least partially, upstream of PKA.

Because the effects of 6-Bnz-cAMP are global and to determine whether Adcy6 activity is required in SC following PKA activation, we injected *sox10:PKA*^{act} construct in *adcy6a*$^{-/-}$*; adcy6b*$^{-/-}$ embryos. This promoter driven construct allows the expression of a constitutively active form of PKA (PKA^{act})[30] under the control of *sox10* promoter, which is expressed in SC and neural crest[32]. When expressed into *adcy6a*$^{-/-}$*; adcy6b*$^{-/-}$ embryos, *sox10:PKA*^{act} was able to significantly enhance *mbp* expression along the PLLn and shifted the distribution of the phenotypic classes in comparison to control *adcy6a*$^{-/-}$*; adcy6b*$^{-/-}$ embryos expressing only a *sox10:EGFP* construct (Figure 6D).

These results suggest that PKA is an important effector of Gpr126/Adcy6 signaling that functions downstream of Adcy6 in SC *in vivo* to induce early myelin gene expression.

Adcy6 regulates PLLg development and axonal transport along the PLLn *in vivo* in zebrafish

No sign of axonal degeneration was observed in the PLLn of *adcy6a*$^{-/-}$*; adcy6b*$^{-/-}$ zebrafish embryos or in the sciatic nerves of *Adcy5*$^{-/-}$ *Adcy6*$^{-/-}$ mice, and to understand the decrease in the

total number of axons, we first analyzed the number of neuronal cell bodies in the posterior lateral line ganglion (PLLg) of zebrafish embryos at 48hpf and 72hpf using the HuC antibody (Figure 7A). We observed a significant decrease in the number of PLLg neurons in *adcy6a*$^{-/-}$*; adcy6b*$^{-/-}$ embryos in comparison to WT embryos at 48hpf and 72hpf, while acridine orange staining, which labels apoptotic cells, was comparable between the two groups (Figure 7B and Figures S5-S6). We next analyzed axonal growth along the PLLn. Whole mount acetylated tubulin immunostaining revealed no significant difference between WT and *adcy6a*$^{-/-}$*; adcy6b*$^{-/-}$ embryos at 48hpf, indicating normal and timely axonal growth (Figure 7C,D). A previous study highlighted a role for cAMP in promoting axonal transport of mitochondria in drosophila wing neurons[33], we therefore explored a possible role for Adcy6 in peripheral axonal transport. For this, we injected *mito:GFP* mRNA and tracked mitochondrial movement along the PLLn using time-lapse imaging. We measured moving speed, which indicates the displacement of a mitochondria during uninterrupted runs divided by the duration of the runs. We also assessed the flux of mitochondria during a given time along individual axons of the PLLn. Anterograde and retrograde moving mitochondria displayed significantly slower moving speeds in *adcy6a*$^{-/-}$*; adcy6b*$^{-/-}$ embryos in comparison with WT, and some moved abruptly in both directions (Figure 7E,F and Movies S5,S6,S7,S8 and S9). We also observed a significant decrease in mitochondrial flux along individual axons in *adcy6a*$^{-/-}$*; adcy6b*$^{-/-}$ embryos (Figure 7F).
These results show that Adcy6 activity is required for neuronal development and axonal transport, but is dispensable for axonal outgrowth.

Adcy6 functions within neurons to regulate NaCh clustering along the PLLn *in vivo*

Since ion channels accumulate at the nodes of Ranvier via axonal transport[34], we wondered whether Adcy6 regulates clustering of voltage-gated sodium channels within the nodes. Whole mount immunofluorescence analysis using monoclonal antibody that recognizes all voltage-gated sodium channels shows a significant decrease in the number of NaCh clusters in *adcy6a*$^{-/-}$*; adcy6b*$^{-/-}$ embryos in comparison with WT (Figure 8A,B). Moreover, whereas clusters of NaCh were evenly distributed along the antero-posterior axis of the PLLn in WT embryos (ratio=1), the ratio was significantly increased in *adcy6a*$^{-/-}$*; adcy6b*$^{-/-}$ embryos, suggesting a decrease in NaCh clustering in the posterior region when compared to a more anterior region of the PLLn (Figure 8C,D).
To determine whether the decreased NaCh clustering resulted from a decrease in the number of myelinated axons or was due to a defect in axonal transport, we chose to specifically manipulate Adcy6 function in the PLLg. In order to do so, we first used *adcy6a/b* MOs, which

were previously designed and tested[15] and which phenocopy the *adcy6a*$^{-/-}$*; adcy6b*$^{-/-}$ mutant, because it was not possible to have enough mutant chimeras to statistically validate results. We quantified the number of nodes of Ranvier within the PLLn in a given area and counted an average of 9.5 nodes of Ranvier in WT axons (n= 6 embryos), whereas we found only 1.33 nodes in *adcy6a/b* morphants (n= 6 embryos) (Figure 8E,F). We then generated mosaic PLLg of WT and *adcy6a/b* morphant cells by introducing *adcy6a/b* morphant cells, co-injected with *mCherry* mRNA into a WT background. In such chimeras, no or very few sodium channel clustering (0.66±0.47 clusters per area) was observed along the PLLn axons derived from *adcy6a/b* axons (3 different embryos) (Figure 8E), while sodium channel clustering was observed in surrounding axons expressing normal levels of Adcy6. We then introduced WT cells, labelled with *mCherry,* into *adcy6a/b* morphant embryos (3 different embryos). In this case, we observed normal sodium channel clustering along the axons (3±0.81 clusters per area) (Figure 8E), while surrounding axons show little or no sign of sodium channel clustering.
These results indicate that Adcy6 activity is required within neurons and contributes to the clustering of NaCh along peripheral axons.

Discussion

Several studies have established a fundamental role for cAMP in SC development and myelination *in vitro*, dating back to as early as 1980s[8,9,35]. *In vitro* cAMP elevation, and *in vivo* forskolin treatment, that activates adenyl cyclase and elevates cAMP, can trigger the up-regulation of myelin proteins and the differentiation of SC[12,27,31,36]. However, the molecular mechanism that activates cAMP in the PNS, and its broad role in peripheral nerve development and the linear development of SC remains unknown. We have previously identified mutations in *ADCY6* as responsible for severe AMC with peripheral myelin defects, showing the first piece of evidence that ADCY6 impacts upon peripheral myelination[37]. In this study, using genetic and pharmacological approaches, as well as live imaging in two complementary vertebrate models, we identify Adcy6, albeit in synergy with Adcy5 in mice, as a novel key regulator of both neuronal/axonal development and timely sheath growth in the PNS of vertebrates.

Impaired timely radial sorting and sheath growth: Link to Gpr126 and PKA

Abnormal axonal radial sorting in *Adcy5*$^{-/-}$ *Adcy6*$^{lox/lox}$ *MPZ*$^{cre+}$, *Adcy5*$^{-/-}$ *Adcy6*$^{-/-}$ mice and zebrafish *adcy6a*$^{-/-}$*; adcy6b*$^{-/-}$ mutants suggests that Adcy6 affects timely SC radial sorting and myelination. This result is reminiscent of *Gpr126*$^{-/-}$, whereby GPR126 facilitates the link

between the extracellular environment, more specifically Laminin-211, and SC myelination via cAMP[18]. It is therefore possible that Adcy6 is one of the missing links that associates Gpr126 activity with cAMP accumulation, at least at the early stages. Indeed, our *in vivo* genetic interaction analysis in zebrafish, provides evidence that Gpr126 primarily relies on Adcy6, to promote early SC myelin gene expression, upstream of PKA.

Gpr126$^{-/-}$, *Adcy5*$^{-/-}$ *Adcy6*$^{lox/lox}$ *MPZ*$^{cre+}$, *Adcy5*$^{-/-}$ *Adcy6*$^{-/-}$ mice and zebrafish *adcy6a*$^{-/-}$*; adcy6b*$^{-/-}$ mutants eventually recover and sort axons, however, Gpr126 remains essential for myelination by SC until adulthood. Even though adult *Adcy5*$^{-/-}$ *Adcy6*$^{lox/lox}$ *MPZ*$^{cre+}$ and *Adcy5*$^{-/-}$ *Adcy6*$^{-/-}$ mice present a significant decrease in the number of myelinated axons, some myelin formation takes place in the absence of Adcy6, unlike Gpr126 mutants. This result reveals i) a critical role for Adcy6 for timely myelin formation and ii) that other adenyl cyclases might compensate the absence of Adcy6 allowing some myelination to proceed at later stages.

In contrast to zebrafish and humans, *Adcy6*$^{-/-}$ mice survive to adulthood with no gross morphological defects. Although the removal of Adcy6 delays myelin formation at P5 and P10 and *Adcy5*$^{-/-}$ has no impact upon myelin formation in mice, the elimination of both proteins produces a significant delay in myelin formation, among other peripheral nerve defects. This indicates: i) a functional synergistic interaction between the two proteins specifically in mice and ii) that Adcy6 is the primary adenyl cyclase required for timely peripheral myelination in vertebrates.

Our marker studies indicate that the early steps of SC distribution along PLLn and proliferation are normal in *adcy6a*$^{-/-}$*; adcy6b*$^{-/-}$ mutants. Moreover, TEM and RT-qPCR analyses show that SC are temporarily blocked at the promyelinating stage in zebrafish and mice. While *Sox10* expression is comparable between all groups at P5 and P10, *Krox20* as well as markers of differentiated SC, such as *Mbp* and *Mpz* are significantly decreased at these developmental stages. This phenotype recalls the early phenotypes of *Gpr126* mutants, in which SC stall at promyelinating stage and are unable to myelinate[12–14].

Adcy6 in neuronal and axonal development

Interestingly, *Adcy5*$^{-/-}$ *Adcy6*$^{-/-}$ mice and zebrafish *adcy6a*$^{-/-}$*; adcy6b*$^{-/-}$ mutants show a significant decrease in the total number of axons compared with WT nerves. This result is comparable with Gpr126 mutants [13], but these defects were never assessed in constitutive *Gpr126*$^{-/-}$ mice mutants. It is important to note that *adcy6a*$^{-/-}$*; adcy6b*$^{-/-}$ mutants show no significant defect in PLLn axonal growth, neither in SC proliferation and numbers, discarding a general developmental delay in *adcy6a*$^{-/-}$*; adcy6b*$^{-/-}$ mutants. Moreover, we observe no axonal

degeneration in TEM in *adcy6a*$^{-/-}$*; adcy6b*$^{-/-}$ mutants and *Adcy5*$^{-/-}$ *Adcy6*$^{-/-}$ mice. On the other hand, we observe a significant decrease in the number of neurons within the PLLg at different stages, providing evidence that Adcy6 impacts upon neuronal development. Several studies highlighted an important role for cAMP in neuronal differentiation[38–41]; it is possible that Adcy6 is the primary adenyl cyclase that activates cAMP and promote neuronal differentiation within the PNS.

We also observe a significant decrease in mitochondrial axonal transport along the axons, that is likely to contribute to the significant decrease in the clustering of NaCh along the antero-posterior axis of the PLLn. Indeed, ion channels and cytoskeletal components accumulate at the nodes via axonal transport[34], and our data show that Adcy6 functions autonomously in neurons to mediate sodium channel clustering. It has been shown that the cAMP/PKA/Kinesin-1 pathway promotes the axonal transport of mitochondria in the Drosophila wing nerve system[33]. Thus, it is likely that Adcy6 activity impacts upon cAMP to promote axonal transport along peripheral axons in vertebrates.

Adcy6 regulates several aspects of peripheral nerve development

Combining mice and zebrafish data, we hereby provide evidence of a fundamental role for Adcy6 in driving timely myelination by SC in vertebrates, along with a key role in neuronal/axonal development that impacts upon sodium channel clustering. These observations indicate that Adcy6 has important functions in multiple cells types within the PNS. While Adcy6, in synergy with Adcy5 in mice, functions autonomously within SCs for timely peripheral myelination, we suggest that a blend of several defects including: i) reduction in nerve size, ii) axonal transport defect, iii) defective clustering of NaCh within the nodes and iv) significant decrease in the number of myelinated axons, contribute to nerve conduction dysfunction along peripheral axons and the development of peripheral neuropathy.

Interestingly, a significant percentage of axons show a substantial increase in their diameters (>7µm) that is likely to result from the significant delay in early myelin development in *Adcy5*$^{-/-}$ *Adcy6*$^{lox/lox}$ *MPZ*$^{cre+}$ sciatic nerves, in comparison with *Adcy5*$^{-/-}$ *Adcy6*$^{-/-}$ mice. This is an interesting observation, since one of the major functions of myelin sheath from an evolutionary point of view, is to accelerate the speed of conduction along axons without increasing the diameter of axons[4,42]. Three major components define the axonal cytoskeleton: microtubules, neurofilaments and actin[43] and the crosslinking between neurofilaments and cytoskeletal components leads to an increase of axon diameter[44,45]. Several lines of evidence link cAMP activity to actin-cytoskeletal remodeling and Rho-GTPases, including RhoA and Rac1[46–48], as

well as microtubules function through its ability to phosphorylate microtubule-associated protein 2 (MAP 2)[49] and neurofilament assembly through PKA[50]. It is possible that neuronal Adcy6 activity would impact upon axonal cAMP levels to modulate cytoskeletal components and mediate the increase in axonal diameter to compensate the significant delay in early myelin sheath formation.

Adcy6 activity: links to human disorders

The zebrafish and mice mutants described here provide novel models to study Adcy6 function in vertebrates and further understand its role in human pathology. The lethality and limb phenotype are reminiscent of human patients with AMC[37,51], while peripheral myelin formation defects at early stages were comparable to constitutive *Gpr126*$^{-/-}$ mutants and patients with *ADCY6* and *GPR126* mutations[15,17].

Adenyl cyclase is known to be the primary effector in the ß-adrenergic receptors (ß AR) signaling. More specifically, Adcy5 and Adcy6 are the main adenyl cyclases responsible for cAMP synthesis in cardiomyocytes and show functional redundancy in ßAR-mediated ionotropic response[52]. However, published reports of patients with *ADCY6* mutations do not reveal any clinical feature of heart defects but rather severe feeding difficulties, hypotonia and respiratory failure[53,54]. Taken together, it is likely that respiratory problems, feeding disorders and severe immobility contribute to the lethality of constitutive *Adcy5*$^{-/-}$ *Adcy6*$^{-/-}$ mice, zebrafish *adcy6a*$^{-/-}$*; adcy6b*$^{-/-}$ mutants and patients with *ADCY6* mutations.

It is important to note that adenyl cyclases also play a variety of important functions in the CNS[55], such as learning/memory and locomotion. For instance, loss of Adcy3 is associated with depressive disorder in humans[56,57] and loss of Adcy5 results in Parkinson-like motor dysfunction[58]. It is therefore possible that some aspects of adult locomotion defects observed in *Adcy5*$^{-/-}$ *Adcy6*$^{-/-}$ mice and zebrafish *adcy6a*$^{-/-}$*; adcy6b*$^{-/-}$ mutants are related to a loss of function of Adcy6 in the CNS. For instance, adult *adcy6a*$^{-/-}$*; adcy6b*$^{-/-}$ zebrafish mutants present some epileptic seizure behavior, reminiscent of symptoms found in a female patient with *ADCY6* mutation presenting epilepsy and pachygyria[54].

cAMP can impact upon various upon significant physiological processes, ranging from regulatory events to metabolism, proliferation, growth and differentiation. In this regard, understanding the role and specificity of the enzymes that produce the cAMP signal, i.e. adenyl cyclases, would pave the way to strategies for a selective regulation of cAMP signaling; in this context, Adcy6 would represent an attractive target for PNS treatments.

Figure legends

Figure 1- *Adcy6* mutant mice display delayed myelination.

(**A**) Relative expression of *Adcy6* mRNA normalized to Cyclophilin A (*CycloA*) in embryonic mice DRG at E13 (0.8868± 0.226, n=4) and in sciatic nerve at P5 (3.795± 0.1899, n=3).

(**B**) Representative transmission electron microscopy images of ultrathin transverse sections (0.4 μm) of sciatic nerves from control and *Adcy6*$^{-/-}$ mice at P5, P10 and adult stages. *(red): myelinated axon; *(blue): sorted non-myelinated axon; *(white): Schwann cell. Field: 570 μm^2. Scale bar: 2 μm.

(**C**) Myelinated axons per field in sciatic nerves from mice at P5 (control: 23.19 ± 2.107, n=3; *Adcy6* $^{-/-}$: 8.567 ± 1.676, n=3; p=0.0056), P10 (control: 31.53± 1.867, n=4; *Adcy6*$^{-/-}$: 21.65 ± 1.599, n=4; p=0.007) and adult stage (control: 19.29 ± 0.4552, n=3; *Adcy6*$^{-/-}$: 19.63 ± 1.450, n=3). Statistical analyses were performed using the unpaired *t*-test.

(**D**) Total number of axons per field in sciatic nerves from mice at P5 (control: 83.69 ± 13.78, n=3; *Adcy6*$^{-/-}$: 92.26 ± 11.24, n=3), P10 (control: 67.70 ± 9.037, n=4; *Adcy6*$^{-/-}$: 50.42 ± 6.191, n=4) and adult stage (control: 58.21 ± 5.681, n=3; *Adcy6*$^{-/-}$: 59.77 ± 9.173, n=3). Statistical analyses were performed using the unpaired *t*-test.

(**E**) Sorted non-myelinated axons per field in sciatic nerves from mice at P5 (control: 2.922 ± 0.3964, n=3; *Adcy6*$^{-/-}$: 11.40 ± 1.266, n=3; p=0.0031), P10 (control: 0.6829 ± 0.2468, n=4; *Adcy6*$^{-/-}$: 3.210 ± 1.447, n=4; p=0.1360) and adult stage (control: 0 ± 0, n=3; *Adcy6*$^{-/-}$: 0 ± 0, n=3). Statistical analyses were performed using the unpaired *t*-test.

(**F-H**) Proportion of myelinated and unmyelinated axons (1:1) at (**F**) P5 (control: myelinated axons= 89%, unmyelinated axons= 11%, n=3; *Adcy6*$^{-/-}$: myelinated axons= 43%, unmyelinated axons= 57%, n=3; p<0.0001), (**G**) P10 (control: myelinated axons= 98%, unmyelinated axons= 2%, n=4; *Adcy6*$^{-/-}$: myelinated axons= 87%, unmyelinated axons= 13%, n=4; p= 0.3687) and (**H**) adult stage (control: myelinated axons=100%, unmyelinated axons=0% , n=3; *Adcy6*$^{-/-}$: myelinated axons=100%, unmyelinated axons=0% , n=3; p >0.9999). Statistical analyses were performed using the Fischer's exact test.

(**I**) G-ratio analysis of myelinated axons in sciatic nerves from mice at P5 (control: 0.7338 ± 0.009419, n=3; *Adcy6*$^{-/-}$: 0.7531 ± 0.01866, n=3), P10 (control: 0.6641 ± 0.02747, n=4; *Adcy6*$^{-/-}$: 0.7017 ± 0.01188, n=4) and adult stage (control: 0.6801 ± 0.01105, n=3; *Adcy6*$^{-/-}$: 0.7571 ± 0.05782, n=3). Statistical analyses were performed using the unpaired *t*-test.

(**C**-**I**) Results represent the average of 10 fields analyzed per sciatic nerve.

(**J**-**L**) Relative expression of Schwann cell and myelin markers normalized to Cyclophilin A in sciatic nerves from control and *Adcy6*$^{-/-}$ mice at (**J**) P5 (control: n=8; *Adcy6*$^{-/-}$: n=5; *Mpz*: p= 0.0050; *Pmp22*: p= 0.0070 and *Mbp*: p= 0.0054), (**K**) P10 (control: n=4; *Adcy6*$^{-/-}$: n=4; *Mpz*: p=0.0630; *Pmp22*: p= 0.0762 and *Mbp*: p= 0.0666) and (**L**) adult stage (control: n=6; *Adcy6*$^{-/-}$: n=4) analyzed by RT-qPCR. Statistical analyses were performed using an unpaired *t*-test or the Mann-Whitney test, as appropriate.

(**M**) Representative transmission electron microscopy images of ultrathin transverse sections (0.4 μm) of sciatic nerves from control and *Adcy6*$^{lox/lox}$ *MPZ*$^{cre+}$ mice at P5 and adult stages. *(red): myelinated axon; *(white): Schwann cell. Field: 570 μm^2 (P5) and 1592.81 μm^2 (adults). Scale bar: 2 μm.

(**N**) Myelinated axons per field in sciatic nerves from mice at P5 (control: 20.93$\pm$ 1.678, n=4; *Adcy6*$^{lox/lox}$ *MPZ*$^{cre+}$: 17.60$\pm$ 1.848, n=3) and adult stage (control: 38.37 $\pm$ 0.4910, n=3; *Adcy6*$^{lox/lox}$ *MPZ*$^{cre+}$: 41.20 $\pm$ 6.608, n=3). Statistical analyses were performed using the unpaired *t*-test.

(**O**) G-ratio analysis of myelinated axons in sciatic nerves from mice at P5 (control: 0.7054 $\pm$ 0.014, n=4; *Adcy6*$^{lox/lox}$ *MPZ*$^{cre+}$: 0.7265 $\pm$ 0.018, n=3) and adult stage (control: 0.6965 $\pm$ 0.03221, n=4; *Adcy6*$^{lox/lox}$ *MPZ*$^{cre+}$: 0.6921 $\pm$ 0.008073, n=3). Statistical analyses were performed using an unpaired *t*-test or the Mann-Whitney test, as appropriate.

In (**A**), (**C**-**L**) and (**N**,**O**), bars represent the mean$\pm$SEM and each plot represents the number of mice analyzed (*n*).

Figure 2- *Adcy5*$^{-/-}$ *Adcy6*$^{-/-}$ mice exhibit developmental delay, functional impairments and altered sciatic nerve conduction.

(**A**) Relative expression of *Adcy5* and *Adcy6* mRNA normalized to Cyclophilin A (*CycloA*) in embryonic mice DRG at E13 (*Adcy5:* 0.4413$\pm$ 0.1146, n=4 and *Adcy6:* 0.8868$\pm$ 0.226, n=4) and in sciatic nerve at P5 (*Adcy5:* 0.4596$\pm$ 0.009692, n=3 and *Adcy6:* 3.795$\pm$ 0.1899, n=3).

(**B**) Representative images showing mice with reduced body size and hindlimb defects in *Adcy5*$^{-/-}$ *Adcy6*$^{-/-}$ mouse compared to control one at P5.

(C) Kaplan-Meier survival test of control (n=13) and *Adcy5*$^{-/-}$ *Adcy6*$^{-/-}$ *mice* (n=36) showing a high mortality in mutants compared to their control siblings (χi^2= 10.36, df=1 and p= 0.0013). Statistical significance was assessed using the log-Rank (Mantel-Cox) test.

(**D-F**) Tail suspension test performance. (**D**) Representative images of a control mouse displaying normal hindlimb extension and splaying during the tail suspension test, whereas *Adcy5*$^{-/-}$ *Adcy6*$^{-/-}$ mouse exhibits a hindlimb clasping phenotype with all four limbs flexed toward the body. (**E**) Percentage of the distribution of each behavioral impairment score (0-4) per group (score 0: control: 100±0, n=4; *Adcy5*$^{-/-}$*Adcy6*$^{-/-}$: 41.47±2.366, n=4; p<0.0001; score 1: control: 0±0, n=4; *Adcy5*$^{-/-}$*Adcy6*$^{-/-}$: 4.452± 2.183, n=4; p= 0.0875; score 2: control: 0±0, n=4; *Adcy5*$^{-/-}$*Adcy6*$^{-/-}$: 23.97± 7.435, n=4; p= 0.0180; score 3: control: 0±0, n=4; *Adcy5*$^{-/-}$ *Adcy6*$^{-/-}$: 20.25± 6.495, n=4; p= 0.0206; score 4: control: 0±0, n=4; *Adcy5*$^{-/-}$*Adcy6*$^{-/-}$: 9.854± 9.349, n=4). Statistical significance was assessed using unpaired *t*-test or the Mann-Whitney test, as appropriate. (**F**) Percentage of the time spent displaying defective behavior relative to the total test duration (control: 0±0, n=4; *Adcy5*$^{-/-}$*Adcy6*$^{-/-}$: 58.53±2.366, n=4; p<0.0001). Statistical analyses were performed using unpaired t-test.

(G,H) Pole test performance. (**G**) Representative pole test images showing performance differences in one-month-old mice: the control mouse firmly grasps the pole with his hindlimbs (left), while *Adcy5*$^{-/-}$*Adcy6*$^{-/-}$ mouse fails to engage them properly (right). (**H**) Pole test score (control: 1±0, n=6; *Adcy5*$^{-/-}$: 0.8750±0.1250, n=8; *Adcy6*$^{-/-}$: 0.8333±0.1667, n=6; *Adcy5*$^{-/-}$ *Adcy6*$^{-/-}$: 0±0, n=7; p=0.0011 (control *vs. Adcy5*$^{-/-}$*Adcy6*$^{-/-}$); p=0.0026 (*Adcy5*$^{-/-}$ *vs. Adcy5*$^{-/-}$ *Adcy6*$^{-/-}$); p=0.0109 (*Adcy6*$^{-/-}$ *vs. Adcy5*$^{-/-}$*Adcy6*$^{-/-}$)). Statistical analyses were performed using the Kruskal-Wallis test.

(**I,J**) Motor nerve conduction analysis of the sciatic nerve-gastrocnemius muscle pathway. Following sciatic nerve stimulation compound muscle action potential (CMAP) (**I**) latency and (**J**) duration were recorded. (**I**) CMAP latency in 2-month-old mice (control: 0.8419± 0.05840, n=8; *Adcy5*$^{-/-}$: 1.160± 0.1664, n=5; *Adcy6*$^{-/-}$: 0.8857± 0.07546, n=7; *Adcy5*$^{-/-}$*Adcy6*$^{-/-}$: 1.746± 0.2451, n=5; p=0.0004 (control *vs. Adcy5*$^{-/-}$*Adcy6*$^{-/-}$); p=0.0418 (*Adcy5*$^{-/-}$ *vs. Adcy5*$^{-/-}$*Adcy6*$^{-/-}$); p=0.0009 (*Adcy6*$^{-/-}$ *vs. Adcy5*$^{-/-}$*Adcy6*$^{-/-}$)). (**J**) CMAP duration in the same mice (control: 2.489± 0.1715, n=8; *Adcy5*$^{-/-}$: 2.712± 0.1951, n=5; *Adcy6*$^{-/-}$: 3.144± 0.3503, n=7; *Adcy5*$^{-/-}$*Adcy6*$^{-/-}$: 4.217± 0.3794, n=5; p=0.0017 (control *vs. Adcy5*$^{-/-}$*Adcy6*$^{-/-}$); p=0.0141 (*Adcy5*$^{-/-}$ *vs. Adcy5*$^{-/-}$ *Adcy6*$^{-/-}$); p=0.0735 (*Adcy6*$^{-/-}$ *vs. Adcy5*$^{-/-}$*Adcy6*$^{-/-}$)). Statistical analyses were performed using the one-way ANOVA or the Kruskal-Wallis test, as appropriate. In (**A**), (**E,F**), (**H**) and (**I,J**), bars represent the mean±SEM and each plot represents the number of mice analyzed (*n*).

Figure 3- *Adcy5*$^{-/-}$ *Adcy6*$^{-/-}$ mice display severe myelination defects and a reduced nerve area.

(**A**) Representative images of sciatic nerves in P5 mice which appear more transparent in *Adcy5*$^{-/-}$ *Adcy6*$^{-/-}$ mice *(right)* compared to control *(left)* and show reduced nerve thickness.
(**B**) Representative transmission electron microscopy images of ultrathin transverse sections (0.4 μm) of sciatic nerve from control, *Adcy5*$^{-/-}$, *Adcy6*$^{-/-}$ and *Adcy5*$^{-/-}$*Adcy6*$^{-/-}$ mice at P5, P10 and adult stages. *(red): myelinated axon; *(blue): sorted non-myelinated axon; *(white): Schwann cell. Field: 570 μm^2. Scale bar: 2 μm.
(**C**) Myelinated axons per field in sciatic nerves at P5 (control: 23.19±2.107, n=3; *Adcy5*$^{-/-}$: 20.84±2.868, n=3; *Adcy6*$^{-/-}$: 8.567±1.676, n=3; *Adcy5*$^{-/-}$*Adcy6*$^{-/-}$: 0.025±0.025, n=4; p=0.0016 (control *vs. Adcy6*$^{-/-}$); p <0.0001 (control *vs. Adcy5*$^{-/-}$*Adcy6*$^{-/-}$); p= 0.0291 (*Adcy6*$^{-/-}$ *vs. Adcy5*$^{-/-}$ *Adcy6*$^{-/-}$)), P10 (control: 31.53±1.867, n=4; *Adcy5*$^{-/-}$: 31.76±3.578, n=3; *Adcy6*$^{-/-}$: 21.65±1.599, n=4; *Adcy5*$^{-/-}$*Adcy6*$^{-/-}$: 1.349±1.098, n=4; p=0.0180 (control *vs. Adcy6*$^{-/-}$); p<0.0001 (control *vs. Adcy5*$^{-/-}$*Adcy6*$^{-/-}$); p<0.0001 (*Adcy6*$^{-/-}$ *vs. Adcy5*$^{-/-}$*Adcy6*$^{-/-}$)) and adult stage (control: 19.29± 0.4552, n=3; *Adcy5*$^{-/-}$: 26.57± 2.945, n=3; *Adcy6*$^{-/-}$: 19.63± 1.45, n=3; *Adcy5*$^{-/-}$*Adcy6*$^{-/-}$: 21.2± 1.345, n=3). Statistical analyses were performed using the one-way ANOVA or the Kruskal-Wallis test, as appropriate.
(**D**) Sorted axons per field in sciatic nerves at P5 (control: 26.12± 1.889, n=3; *Adcy5*$^{-/-}$: 24.94± 2.930, n=3; *Adcy6*$^{-/-}$: 19.97± 1.217, n=3; *Adcy5*$^{-/-}$*Adcy6*$^{-/-}$: 8.578± 1.295, n=3; p=0.0004 (control *vs. Adcy5*$^{-/-}$*Adcy6*$^{-/-}$); p=0.0006 (*Adcy5*$^{-/-}$ *vs. Adcy5*$^{-/-}$*Adcy6*$^{-/-}$); p=0.0073 (*Adcy6*$^{-/-}$ *vs. Adcy5*$^{-/-}$*Adcy6*$^{-/-}$)). Statistical analyses were performed using the one-way ANOVA test.
(**E**) Sorted non-myelinated axons per field in sciatic nerves at P5 (control: 2.922±0.3964, n=3; *Adcy5*$^{-/-}$: 4.1±0.4933, n=3; *Adcy6*$^{-/-}$: 11.4±1.266, n=3; *Adcy5*$^{-/-}$*Adcy6*$^{-/-}$: 8.578±1.295, n=4; p=0.0018 (control *vs. Adcy6*$^{-/-}$); p=0.0153 (control *vs. Adcy5*$^{-/-}$*Adcy6*$^{-/-}$)), P10 (control: 0.6829±0.2468, n=4; *Adcy5*$^{-/-}$: 1.644±0.328, n=3; *Adcy6*$^{-/-}$: 3.21±1.447, n=4; *Adcy5*$^{-/-}$*Adcy6*$^{-/-}$: 6.948±0.3573, n=4; p=0.0008 (control *vs. Adcy5*$^{-/-}$*Adcy6*$^{-/-}$)) and adult stage (control: 0± 0, n=3; *Adcy5*$^{-/-}$: 0± 0, n=3; *Adcy6*$^{-/-}$: 0± 0, n=3; *Adcy5*$^{-/-}$*Adcy6*$^{-/-}$: 0.06667± 0.03333, n=3). Statistical analyses were performed using the one-way ANOVA test.
(**F-H**) Proportion of myelinated and unmyelinated axons (1:1) at (**F**) P5 (control: myelinated axons=89%, unmyelinated axons= 11%, n=3; *Adcy5*$^{-/-}$: myelinated axons= 83% , unmyelinated axons= 17%, n=3; *Adcy6*$^{-/-}$: myelinated axons= 43%, unmyelinated axons= 57%, n=3; *Adcy5*$^{-/-}$*Adcy6*$^{-/-}$: myelinated axons= 0%, unmyelinated axons= 100%, n=3; p<0.0001 (control *vs. Adcy6*$^{-/-}$); p<0.0001 (control *vs. Adcy5*$^{-/-}$*Adcy6*$^{-/-}$)), (**G**) P10 (control: myelinated axons= 98%, unmyelinated axons= 2%, n=4; *Adcy5*$^{-/-}$: myelinated axons= 95%, unmyelinated axons= 5%, n=3; *Adcy6*$^{-/-}$: myelinated axons= 87%, unmyelinated axons= 13%, n=4; *Adcy5*$^{-/-}$*Adcy6*$^{-/-}$:

myelinated axons= 12% , unmyelinated axons= 88%, n=4; p<0.0001 (control *vs.* *Adcy5*$^{-/-}$ *Adcy6*$^{-/-}$)) and (**H**) adult stage (control: myelinated axons= 100%, unmyelinated axons= 0%, n=3; *Adcy5*$^{-/-}$: myelinated axons= 100%, unmyelinated axons= 0%, n=3; *Adcy6*$^{-/-}$: myelinated axons= 100%, unmyelinated axons= 0%, n=3; *Adcy5*$^{-/-}$*Adcy6*$^{-/-}$: myelinated axons= 100%, unmyelinated axons= 0%, n=3). Statistical analyses were performed using the Fischer's exact test.

(**I**) G-ratio analysis of myelinated axons in sciatic nerves at P5 (control: 0.7338±0.009419, n=3; *Adcy5*$^{-/-}$: 0.7488±0.006115, n=3; *Adcy6*$^{-/-}$: 0.7531±0.01866, n=3; *Adcy5*$^{-/-}$*Adcy6*$^{-/-}$: 0±0, n=4); p<0.0001 (control *vs.* *Adcy5*$^{-/-}$*Adcy6*$^{-/-}$)), P10 (control: 0.6641±0.02747, n=4; *Adcy5*$^{-/-}$: 0.6796±0.02455, n=3; *Adcy6*$^{-/-}$: 0.7017±0.01188, n=4; *Adcy5*$^{-/-}$*Adcy6*$^{-/-}$: 0.7759±0.07871, n=3) and adult stage (control: 0.6801± 0.01105, n=3; *Adcy5*$^{-/-}$: 0.6557± 0.01229, n=3; *Adcy6*$^{-/-}$: 0.7571± 0.05782, n=3; *Adcy5*$^{-/-}$*Adcy6*$^{-/-}$: 0.7387± 0.01700, n=3). Statistical analyses were performed using the one-way ANOVA test.

(**J**) Number of total axons per field in sciatic nerves at P5 (control: 83.69±13.78, n=3; *Adcy5*$^{-/-}$: 67.32±6.407, n=3; *Adcy6*$^{-/-}$: 92.26±11.24, n=3; *Adcy5*$^{-/-}$*Adcy6*$^{-/-}$: 58.62±5.758, n=4), P10 (control: 67.70±9.037, n=4; *Adcy5*$^{-/-}$: 70.65±11.34, n=3; *Adcy6*$^{-/-}$: 50.42±6.191, n=4; *Adcy5*$^{-/-}$ *Adcy6*$^{-/-}$: 35.25±3.923, n=4; p=0.0424 (control *vs.* *Adcy5*$^{-/-}$*Adcy6*$^{-/-}$)) and adult stage (control: 58.21± 5.681, n=3; *Adcy5*$^{-/-}$: 44.57± 3.832, n=3; *Adcy6*$^{-/-}$: 59.77± 9.173, n=3; *Adcy5*$^{-/-}$*Adcy6*$^{-/-}$: 67.27± 4.467, n=3). Statistical analyses were performed using the one-way ANOVA or the Kruskal-Wallis test, as appropriate.

(**K**) Percentage of axons per diameter in adult mice with 1 μm bin width: 0-1 μm, 1-2 μm, 2-3 μm, 3-4 μm, 4-5 μm, 5-6 μm, 6-7 μm and over 7 μm (7+). Statistical analyses were performed using the two-way ANOVA test.

(**C**-**K**) results represent the average of 10 fields analyzed per sciatic nerve.

(**L**) Representative images of semithin transverse sections (1 μm) of sciatic nerve from control, *Adcy5*$^{-/-}$, *Adcy6*$^{-/-}$ and *Adcy5*$^{-/-}$*Adcy6*$^{-/-}$mice at P5 and adult stages. Scale bar: 200 μm.

(**M**) Total number of myelinated axons per nerve at P5 (control: 974.5±134.1, n=4; *Adcy5*$^{-/-}$: 1031±96.29, n=4; *Adcy6*$^{-/-}$: 428.5±47.29, n=4; *Adcy5*$^{-/-}$*Adcy6*$^{-/-}$: 12.00±1.472, n=4; p=0.0035 (control *vs.* *Adcy6*$^{-/-}$); p<0.0001 (control *vs.* *Adcy5*$^{-/-}$*Adcy6*$^{-/-}$)) and adult stage (control: 2896± 246.7, n=3; *Adcy5*$^{-/-}$: 2577± 49.17, n=3; *Adcy6*$^{-/-}$: 2197± 221.5, n=4; *Adcy5*$^{-/-}$*Adcy6*$^{-/-}$: 1550± 232.4, n=5; p=0.0061 (control *vs.* *Adcy5*$^{-/-}$*Adcy6*$^{-/-}$)). Statistical analyses were performed using the one-way ANOVA test.

(**N**) Sciatic nerve area at P5 (control: 10.28± 0.5987, n=4; *Adcy5*$^{-/-}$: 8.660± 0.9692, n=4; *Adcy6*$^{-/-}$: 6.714± 0.8226, n=4; *Adcy5*$^{-/-}$*Adcy6*$^{-/-}$: 5.736± 0.5986, n=4; p=0.0279 (control *vs.* *Adcy6*$^{-/-}$); p= 0.0057 (control *vs.* *Adcy5*$^{-/-}$*Adcy6*$^{-/-}$)) and adult stage (control: 29.75± 2.621, n=8; *Adcy5*$^{-/-}$: 27.59± 2.884, n=5; *Adcy6*$^{-/-}$: 29.92± 4.828, n=5; *Adcy5*$^{-/-}$*Adcy6*$^{-/-}$: 11.82± 1.809, n=7; p= 0.00789 *Adcy5*$^{-/-}$ vs. *Adcy5*$^{-/-}$ *Adcy6*$^{-/-}$); p= 0.0023 (*Adcy6*$^{-/-}$ vs. *Adcy5*$^{-/-}$ *Adcy6*$^{-/-}$); p=0.0007 (control *vs.* *Adcy5*$^{-/-}$*Adcy6*$^{-/-}$)). Statistical analyses were performed using the one-way ANOVA test.

(**O-Q**) Relative expression of Schwann cell and myelin markers normalized to Cyclophilin A (*CycloA*) in sciatic nerves from mice at (**O**) P5 (control: n=8; *Adcy5*$^{-/-}$: n=5; *Adcy6*$^{-/-}$: n=5; *Adcy5*$^{-/-}$*Adcy6*$^{-/-}$*:* n=5*; Oct6: p*=0.0675 (control *vs.* *Adcy5*$^{-/-}$*Adcy6*$^{-/-}$); *Krox20: p*=0.0048 (control *vs.* *Adcy5*$^{-/-}$*Adcy6*$^{-/-}$); *Mpz*: p=0.0141 (control *vs.* *Adcy6*$^{-/-}$), p=0.0003 (control *vs.* *Adcy5*$^{-/-}$*Adcy6*$^{-/-}$); *Pmp22*: p=0.0184 (control *vs.* *Adcy6*$^{-/-}$), p=0.0003 (control *vs.* *Adcy5*$^{-/-}$*Adcy6*$^{-/-}$) and *Mbp*: p=0.0030 (control *vs.* *Adcy6*$^{-/-}$), p <0.0001 (control *vs.* *Adcy5*$^{-/-}$*Adcy6*$^{-/-}$)), (**P**) P10 (control: n=4; *Adcy5*$^{-/-}$: n=5; *Adcy6*$^{-/-}$: n=4 and *Adcy5*$^{-/-}$*Adcy6*$^{-/-}$*:* n=6; *Krox20:* p=0.0365(control *vs.* *Adcy5*$^{-/-}$*)*; p=0.0048 (control *vs.* *Adcy5*$^{-/-}$*Adcy6*$^{-/-}$); *Mpz*: p=0.0005 (control *vs.* *Adcy5*$^{-/-}$*Adcy6*$^{-/-}$); *Pmp22*: p=0.0002 (control *vs.* *Adcy5*$^{-/-}$*Adcy6*$^{-/-}$) and *Mbp*: p=0.0620 (control *vs.* *Adcy6*$^{-/-}$); p<0.0001 (control *vs.* *Adcy5*$^{-/-}$*Adcy6*$^{-/-}$)) and (**Q**) adult stage (control: n=6; *Adcy5*$^{-/-}$: n=6; *Adcy6*$^{-/-}$: n=4; *Adcy5*$^{-/-}$*Adcy6*$^{-/-}$*:* n=4; *Sox10*: p=0.0182 (control *vs.* *Adcy5*$^{-/-}$*Adcy6*$^{-/-}$); *Oct6*: p=0.0001 (*Adcy5*$^{-/-}$ *vs.* *Adcy5*$^{-/-}$*Adcy6*$^{-/-}$); p=0.0017 (*Adcy6*$^{-/-}$ *vs.* *Adcy5*$^{-/-}$*Adcy6*$^{-/-}$); p=0.0002 (control *vs.* *Adcy5*$^{-/-}$*Adcy6*$^{-/-}$)) analyzed by RT-qPCR. Statistical analyses were performed using one-way ANOVA or Kruskal-Wallis test, as appropriate.

In (**C-E**), (**I-K**) and (**M-Q**), bars represent the mean±SEM and each plot represents the number of mice analyzed (*n*).

Figure 4- ***Adcy5*$^{-/-}$** ***Adcy6*$^{lox/lox}$** ***MPZ*$^{cre+}$** **mice show normal development, motor activity and nerve conduction but present myelination defects and enlarged axon diameters.**

(**A)** Representative transmission electron microscopy images of ultrathin transverse sections (0.4 μm) of sciatic nerves from control, *Adcy5*$^{-/-}$*Adcy6*$^{-/-}$ and *Adcy5*$^{-/-}$ *Adcy6*$^{lox/lox}$ *MPZ*$^{cre+}$ mice at P5, P10 and adult stages. *(red): myelinated axon; *(blue): sorted non-myelinated axon; *(white): Schwann cell. Field: 570 μm^2. Scale bar: 2 μm.

(**B**) Myelinated axons per field in sciatic nerves at P5 (control: 23.19±2.107, n=3; *Adcy5*$^{-/-}$ *Adcy6*$^{-/-}$: 0.025±0.025, n=4; *Adcy5*$^{-/-}$ *Adcy6*$^{lox/lox}$ *MPZ*$^{cre+}$: 5.320± 0.2676, n=3 ; p <0.0001 (control *vs.* *Adcy5*$^{-/-}$*Adcy6*$^{-/-}$); p <0.0001 (control *vs.* *Adcy5*$^{-/-}$ *Adcy6*$^{lox/lox}$ *MPZ*$^{cre+}$), P10 (control:

31.53±1.867, n=4; *Adcy5*$^{-/-}$*Adcy6*$^{-/-}$: 1.349±1.098, n=4; *Adcy5*$^{-/-}$ *Adcy6*$^{lox/lox}$ *MPZ*$^{cre+}$: 8.397± 0.7836, n=4; p <0.0001 (control *vs.* *Adcy5*$^{-/-}$*Adcy6*$^{-/-}$); p <0.0001 (control *vs.* *Adcy5*$^{-/-}$ *Adcy6*$^{lox/lox}$ *MPZ*$^{cre+}$) and adult stage (control: 19.29± 0.4552, n=3; *Adcy5*$^{-/-}$*Adcy6*$^{-/-}$: 21.2± 1.345, n=3; *Adcy5*$^{-/-}$ *Adcy6*$^{lox/lox}$ *MPZ*$^{cre+}$: 11.07± 0.2906, n=3; p= 0.0011(control *vs.* *Adcy5*$^{-/-}$ *Adcy6*$^{lox/lox}$ *MPZ*$^{cre+}$); p= 0.0003 (*Adcy5*$^{-/-}$*Adcy6*$^{-/-}$ *vs.* *Adcy5*$^{-/-}$ *Adcy6*$^{lox/lox}$ *MPZ*$^{cre+}$)). Statistical analyses were performed using the one-way ANOVA test.

(**C**) Sorted axons per field in sciatic nerves at P5 (control: 26.12±1.889, n=3; *Adcy5*$^{-/-}$*Adcy6*$^{-/-}$: 8.578±1.295, n=4; *Adcy5*$^{-/-}$ *Adcy6*$^{lox/lox}$ *MPZ*$^{cre+}$: 18.64±1.515, n=3; p=0.0002 (control *vs.* *Adcy5*$^{-/-}$*Adcy6*$^{-/-}$); p=0.0328 (control *vs.* *Adcy5*$^{-/-}$ *Adcy6*$^{lox/lox}$ *MPZ*$^{cre+}$); p= 0.0055 (*Adcy5*$^{-/-}$ *Adcy6*$^{-/-}$ *vs.* *Adcy5*$^{-/-}$ *Adcy6*$^{lox/lox}$ *MPZ*$^{cre+}$)). Statistical analyses were performed using the one-way ANOVA test.

(**D**) Sorted non-myelinated axons per field in sciatic nerves at P5 (control: 2.922±0.3964, n=3; *Adcy5*$^{-/-}$*Adcy6*$^{-/-}$: 8.578±1.295, n=4; *Adcy5*$^{-/-}$ *Adcy6*$^{lox/lox}$ *MPZ*$^{cre+}$: 13.32±1.668, n=3; p=0.0360 (control *vs.* *Adcy5*$^{-/-}$*Adcy6*$^{-/-}$); p=0.0023 (control *vs.* *Adcy5*$^{-/-}$ *Adcy6*$^{lox/lox}$ *MPZ*^{cre})), P10 (control: 0.6829±0.2468, n=4; *Adcy5*$^{-/-}$*Adcy6*$^{-/-}$: 6.948±0.3573, n=4; *Adcy5*$^{-/-}$ *Adcy6*$^{lox/lox}$ *MPZ*$^{cre+}$: 9.006±1.494, n=4; p=0.0021 (control *vs.* *Adcy5*$^{-/-}$*Adcy6*$^{-/-}$); p=0.0003 (control *vs.* *Adcy5*$^{-/-}$ *Adcy6*$^{lox/lox}$ *MPZ*^{cre})) and adult stage (control: 0±0, n=3; *Adcy5*$^{-/-}$*Adcy6*$^{-/-}$: 0.06667±0.03333, n=3; *Adcy5*$^{-/-}$ *Adcy6*$^{lox/lox}$ *MPZ*$^{cre+}$: 0.06667±0.03333, n=3). Statistical analyses were performed using the one-way ANOVA or the Kruskal-Wallis test, as appropriate.

(**E-G**) Proportion of myelinated and unmyelinated axons (1:1) at (**E**) P5 (control: myelinated axons=89%, unmyelinated axons= 11%, n=3; *Adcy5*$^{-/-}$*Adcy6*$^{-/-}$: myelinated axons= 0%, unmyelinated axons= 100%, n=3; *Adcy5*$^{-/-}$ *Adcy6*$^{lox/lox}$ *MPZ*$^{cre+}$: myelinated axons= 29%, unmyelinated axons= 71%, n=3; p<0.0001 (control *vs.* *Adcy5*$^{-/-}$*Adcy6*$^{-/-}$); p<0.0001 (control *vs.* *Adcy5*$^{-/-}$ *Adcy6*$^{lox/lox}$ *MPZ*$^{cre+}$)), (**F**) P10 (control: myelinated axons= 98%, unmyelinated axons= 2%, n=4; *Adcy5*$^{-/-}$*Adcy6*$^{-/-}$: myelinated axons= 12%, unmyelinated axons= 88%, n=4; *Adcy5*$^{-/-}$ *Adcy6*$^{lox/lox}$ *MPZ*$^{cre+}$: myelinated axons= 49%, unmyelinated axons= 51%, n=4; p<0.0001 (control *vs.* *Adcy5*$^{-/-}$*Adcy6*$^{-/-}$); p<0.0001 (control *vs.* *Adcy5*$^{-/-}$ *Adcy6*$^{lox/lox}$ *MPZ*$^{cre+}$)) and (**G**) adult stage (control: myelinated axons= 100%, unmyelinated axons= 0%, n=3; *Adcy5*$^{-/-}$*Adcy6*$^{-/-}$: myelinated axons= 100%, unmyelinated axons= 0%, n=3; *Adcy5*$^{-/-}$ *Adcy6*$^{lox/lox}$ *MPZ*$^{cre+}$: myelinated axons= 99%, unmyelinated axons= 1%, n=4). Statistical analyses were performed using the Fischer's exact test.

(**H-J**) Relative expression of Schwann cell and myelin markers normalized to Cyclophilin A (*CycloA*) in sciatic nerves from mice at (**H**) P5 (control: n=8; *Adcy5*$^{-/-}$*Adcy6*$^{-/-}$*:* n=5*; Adcy5*$^{-/-}$

Adcy6$^{lox/lox}$ *MPZ*$^{cre+}$: n=6; *Oct6:* p=0.0732 (control *vs. Adcy5*$^{-/-}$*Adcy6*$^{-/-}$); p= 0.0867 (control *vs. Adcy5*$^{-/-}$ *Adcy6*$^{lox/lox}$ *MPZ*$^{cre+}$); *Krox20*: p=0.0027 (control *vs. Adcy5*$^{-/-}$*Adcy6*$^{-/-}$); p=0.0323 (control *vs. Adcy5*$^{-/-}$ *Adcy6*$^{lox/lox}$ *MPZ*$^{cre+}$); *Mpz*: p<0.0001 (control *vs. Adcy5*$^{-/-}$*Adcy6*$^{-/-}$); p<0.0001 (control *vs. Adcy5*$^{-/-}$ *Adcy6*$^{lox/lox}$ *MPZ*$^{cre+}$); *Pmp22*: p<0.0001 (control *vs. Adcy5*$^{-/-}$ *Adcy6*$^{-/-}$); p<0.0001 (control *vs. Adcy5*$^{-/-}$ *Adcy6*$^{lox/lox}$ *MPZ*$^{cre+}$) and *Mbp*: p<0.0001 (control *vs. Adcy5*$^{-/-}$*Adcy6*$^{-/-}$); p<0.0001 (control *vs. Adcy5*$^{-/-}$ *Adcy6*$^{lox/lox}$ *MPZ*$^{cre+}$)), (**I**) P10 (control: n=4; *Adcy5*$^{-/-}$*Adcy6*$^{-/-}$*:* n=6; *Adcy5*$^{-/-}$ *Adcy6*$^{lox/lox}$ *MPZ*$^{cre+}$: n=4; *Oct6*: p=0.0430 (control *vs. Adcy5*$^{-/-}$ *Adcy6*$^{lox/lox}$ *MPZ*$^{cre+}$); *Krox20:* p=0.0038 (control *vs. Adcy5*$^{-/-}$*Adcy6*$^{-/-}$); *Mpz*: p<0.0001 (control *vs. Adcy5*$^{-/-}$*Adcy6*$^{-/-}$); p<0.0001 (control *vs. Adcy5*$^{-/-}$ *Adcy6*$^{lox/lox}$ *MPZ*$^{cre+}$); *Pmp22*: p<0.0001 (control *vs. Adcy5*$^{-/-}$*Adcy6*$^{-/-}$); p<0.0001 (control *vs. Adcy5*$^{-/-}$ *Adcy6*$^{lox/lox}$ *MPZ*$^{cre+}$) and *Mbp*: p<0.0001 (control *vs. Adcy5*$^{-/-}$*Adcy6*$^{-/-}$); p<0.0001 (control *vs. Adcy5*$^{-/-}$ *Adcy6*$^{lox/lox}$ *MPZ*$^{cre+}$)) and (**J**) adults (control: n=5; *Adcy5*$^{-/-}$*Adcy6*$^{-/-}$*:* n=4; *Adcy5*$^{-/-}$ *Adcy6*$^{lox/lox}$ *MPZ*$^{cre+}$: n=3; *Oct6*: p=0.0032 (control *vs. Adcy5*$^{-/-}$*Adcy6*$^{-/-}$)) analyzed by RT-qPCR. Statistical analyses were performed using one-way ANOVA or Kruskal-Wallis test, as appropriate.

(**K**) Number of total axons per field in sciatic nerves at P5 (control: 83.69±13.78, n=3; *Adcy5*$^{-/-}$*Adcy6*$^{-/-}$: 58.62±5.758, n=4; *Adcy5*$^{-/-}$ *Adcy6*$^{lox/lox}$ *MPZ*$^{cre+}$: 52.86± 5.336, n=3), P10 (control: 67.70±9.037, n=4; *Adcy5*$^{-/-}$*Adcy6*$^{-/-}$: 35.25±3.923, n=4; *Adcy5*$^{-/-}$ *Adcy6*$^{lox/lox}$ *MPZ*$^{cre+}$: 38.11± 2.127, n=4; p= 0.0086 (control *vs. Adcy5*$^{-/-}$*Adcy6*$^{-/-}$); p= 0.0144 (control *vs. Adcy5*$^{-/-}$ *Adcy6*$^{lox/lox}$ *MPZ*^{cre})) and adult stage (control: 58.21± 5.681, n=3; *Adcy5*$^{-/-}$*Adcy6*$^{-/-}$: 67.27± 4.467, n=3; *Adcy5*$^{-/-}$ *Adcy6*$^{lox/lox}$ *MPZ*$^{cre+}$: 32.17± 2.293, n=3). Statistical analyses were performed using the one-way ANOVA or the Kruskal-Wallis test, as appropriate.

(**L**) Percentage of axons per diameter in adult mice with 1 μm bin width: 0-1 μm, 1-2 μm, 2-3 μm, 3-4 μm, 4-5 μm, 5-6 μm, 6-7 μm and over 7 μm (7+). A significative decrease was observed in very small caliber axons (0-1 μm) in *Adcy5*$^{-/-}$ *Adcy6*$^{lox/lox}$ *MPZ*$^{cre+}$ (p <0.0001 (control *vs. Adcy5*$^{-/-}$ *Adcy6*$^{lox/lox}$ *MPZ*^{cre}); p=0.0023 (*Adcy5*$^{-/-}$*Adcy6*$^{-/-}$ *vs. Adcy5*$^{-/-}$ *Adcy6*$^{lox/lox}$ *MPZ*^{cre}) and a significant increase in large caliber axons (7+ μm) (p=0.0081 (control *vs. Adcy5*$^{-/-}$ *Adcy6*$^{lox/lox}$ *MPZ*^{cre}); p=0.0087 (*Adcy5*$^{-/-}$*Adcy6*$^{-/-}$ *vs. Adcy5*$^{-/-}$ *Adcy6*$^{lox/lox}$ *MPZ*^{cre})). Statistical analyses were performed using the two-way ANOVA test.

(**M**) G-ratio analysis of myelinated axons in sciatic nerves at P5 (control: 0.7338±0.009419, n=3; *Adcy5*$^{-/-}$*Adcy6*$^{-/-}$: 0±0, n=4); *Adcy5*$^{-/-}$ *Adcy6*$^{lox/lox}$ *MPZ*$^{cre+}$: 0.7828±0.02221, n=3; p<0.0001 (control *vs. Adcy5*$^{-/-}$*Adcy6*$^{-/-}$); p<0.0001 (control *vs. Adcy5*$^{-/-}$ *Adcy6*$^{lox/lox}$ *MPZ*^{cre})), P10 (control: 0.6641±0.02747, n=4; *Adcy5*$^{-/-}$*Adcy6*$^{-/-}$: 0.7759±0.07871, n=3; *Adcy5*$^{-/-}$ *Adcy6*$^{lox/lox}$ *MPZ*$^{cre+}$: 0.7362± 0.01074, n=4) and adult stage (control: 0.6801± 0.01105, n=3; *Adcy5*$^{-/-}$

Adcy6$^{-/-}$: 0.7387± 0.01700, n=3; *Adcy5*$^{-/-}$ *Adcy6*$^{lox/lox}$ *MPZ*$^{cre+}$: 0.7321± 0.01169, n=4). Statistical analyses were performed using the one-way ANOVA test.

(**B-G**) and (**K-M**) results represent the average of 10 fields analyzed per sciatic nerve.

(**N**) Representative images of semithin transverse sections (1 μm) of sciatic nerves from control, *Adcy5*$^{-/-}$*Adcy6*$^{-/-}$ and *Adcy5*$^{-/-}$ *Adcy6*$^{lox/lox}$ *MPZ*$^{cre+}$ mice at P5 and adult stages. Scale bar: 200 μm.

(**O**) Total number of myelinated axons per nerve at P5 (control: 974.5±134.1, n=4; *Adcy5*$^{-/-}$ *Adcy6*$^{-/-}$: 12.00±1.472, n=4; *Adcy5*$^{-/-}$ *Adcy6*$^{lox/lox}$ *MPZ*$^{cre+}$: 294.0±13.34, n=4; p<0.0001 (control *vs.* *Adcy5*$^{-/-}$*Adcy6*$^{-/-}$); p=0.0004 (control *vs.* *Adcy5*$^{-/-}$ *Adcy6*$^{lox/lox}$ *MPZ*$^{cre+}$)) and adult stage (control: 2896± 246.7, n=3; *Adcy5*$^{-/-}$*Adcy6*$^{-/-}$: 1550± 232.4, n=5; *Adcy5*$^{-/-}$ *Adcy6*$^{lox/lox}$ *MPZ*$^{cre+}$: 1277±151.9, n=4; p= 0.0057 (control *vs.* *Adcy5*$^{-/-}$*Adcy6*$^{-/-}$); p= 0.0024 (control *vs.* *Adcy5*$^{-/-}$ *Adcy6*$^{lox/lox}$ *MPZ*$^{cre+}$)). Statistical analyses were performed using the one-way ANOVA test.

(**P**) Sciatic nerve area at P5 (control: 10.28± 0.5987, n=4; *Adcy5*$^{-/-}$*Adcy6*$^{-/-}$: 5.736± 0.5986, n=4; *Adcy5*$^{-/-}$ *Adcy6*$^{lox/lox}$ *MPZ*$^{cre+}$: 9.831± 1.040, n=4; p= 0.0063 (control *vs.* *Adcy5*$^{-/-}$*Adcy6*$^{-/-}$); p= 0.0116 (*Adcy5*$^{-/-}$*Adcy6*$^{-/-}$ *vs.* *Adcy5*$^{-/-}$ *Adcy6*$^{lox/lox}$ *MPZ*$^{cre+}$)) and adult stage (control: 29.75± 2.621, n=8; *Adcy5*$^{-/-}$*Adcy6*$^{-/-}$: 11.82± 1.809, n=7; *Adcy5*$^{-/-}$ *Adcy6*$^{lox/lox}$ *MPZ*$^{cre+}$: 27.84± 2.265, n=4; p <0.0001 (control *vs.* *Adcy5*$^{-/-}$*Adcy6*$^{-/-}$); p= 0.0017 (*Adcy5*$^{-/-}$*Adcy6*$^{-/-}$ *vs.* *Adcy5*$^{-/-}$ *Adcy6*$^{lox/lox}$ *MPZ*$^{cre+}$)). Statistical analyses were performed using the one-way ANOVA test.

(**Q**) Distribution of the percentage of each behavioral impairment scoring (0-4) per group (score 0: control: 100±0, n=4; *Adcy5*$^{-/-}$*Adcy6*$^{-/-}$: 41.47±2.366, n=4; *Adcy5*$^{-/-}$ *Adcy6*$^{lox/lox}$ *MPZ*$^{cre+}$: 95.35± 1.677, n=4; p<0.0001 (control *vs.* *Adcy5*$^{-/-}$*Adcy6*$^{-/-}$); p<0.0001 (*Adcy5*$^{-/-}$*Adcy6*$^{-/-}$ *vs.* *Adcy5*$^{-/-}$ *Adcy6*$^{lox/lox}$ *MPZ*$^{cre+}$); score 1: control: 0±0, n=4; *Adcy5*$^{-/-}$*Adcy6*$^{-/-}$: 4.452± 2.183, n=4; *Adcy5*$^{-/-}$ *Adcy6*$^{lox/lox}$ *MPZ*$^{cre+}$: 1.111± 1.111, n=4; p= 0.0927 (control *vs.* *Adcy5*$^{-/-}$*Adcy6*$^{-/-}$); score 2: control: 0±0, n=4; *Adcy5*$^{-/-}$*Adcy6*$^{-/-}$: 23.97± 7.435, n=4; *Adcy5*$^{-/-}$ *Adcy6*$^{lox/lox}$ *MPZ*$^{cre+}$: 1.875± 1.875, n=4; p= 0.0134 (control *vs.* *Adcy5*$^{-/-}$*Adcy6*$^{-/-}$); p= 0.0484 (*Adcy5*$^{-/-}$*Adcy6*$^{-/-}$ *vs.* *Adcy5*$^{-/-}$ *Adcy6*$^{lox/lox}$ *MPZ*$^{cre+}$); score 3: control: 0±0, n=4; *Adcy5*$^{-/-}$*Adcy6*$^{-/-}$: 20.25± 6.495, n=4; *Adcy5*$^{-/-}$ *Adcy6*$^{lox/lox}$ *MPZ*$^{cre+}$: 1.659± 1.659, n=4; p= 0.0134 (control *vs.* *Adcy5*$^{-/-}$*Adcy6*$^{-/-}$); p= 0.0484 (*Adcy5*$^{-/-}$*Adcy6*$^{-/-}$ *vs.* *Adcy5*$^{-/-}$ *Adcy6*$^{lox/lox}$ *MPZ*$^{cre+}$); score 4: control: 0±0, n=4; *Adcy5*$^{-/-}$ *Adcy6*$^{-/-}$: 9.854± 9.349, n=4; *Adcy5*$^{-/-}$ *Adcy6*$^{lox/lox}$ *MPZ*$^{cre+}$: 0± 0, n=4). Statistical analyses were performed using one-way ANOVA or Kruskal-Wallis test, as appropriate.

(**R**) Percentage of the time spent displaying defective behavior relative to the total test duration (control: 0±0, n=4; *Adcy5*$^{-/-}$*Adcy6*$^{-/-}$: 58.53±2.366, n=4; *Adcy5*$^{-/-}$ *Adcy6*$^{lox/lox}$ *MPZ*$^{cre+}$: 4.645±

1.677, n=4; p<0.0001 (control *vs. Adcy5*$^{-/-}$*Adcy6*$^{-/-}$); p<0.0001 (*Adcy5*$^{-/-}$*Adcy6*$^{-/-}$ *vs. Adcy5*$^{-/-}$ *Adcy6*$^{lox/lox}$ *MPZ*$^{cre+}$)). Statistical analyses were performed using one-way ANOVA test.

(**S**) Pole test performance of one-month-old mice. Pole test score (control: 1±0, n=6; *Adcy5*$^{-/-}$ *Adcy6*$^{-/-}$: 0±0, n=7; *Adcy5*$^{-/-}$ *Adcy6*$^{lox/lox}$ *MPZ*$^{cre+}$: 0.8333± 0.1667, n=7; p= 0.0012 (control *vs. Adcy5*$^{-/-}$*Adcy6*$^{-/-}$); p=0.0094 (*Adcy5*$^{-/-}$*Adcy6*$^{-/-}$ *vs. Adcy5*$^{-/-}$ *Adcy6*$^{lox/lox}$ *MPZ*$^{cre+}$)). Statistical analyses were performed using the Kruskal-Wallis test.

(**T,U**) Motor nerve conduction analysis of the sciatic nerve-gastrocnemius muscle pathway. Following sciatic nerve stimulation compound muscle action potential (CMAP) (**T**) latency and (**U**) duration were recorded. (**T**) CMAP latency in 2-month-old mice (control: 0.8419± 0.05840, n=8; *Adcy5*$^{-/-}$*Adcy6*$^{-/-}$: 1.746± 0.2451, n=5; *Adcy5*$^{-/-}$ *Adcy6*$^{lox/lox}$ *MPZ*$^{cre+}$: 1.090± 0.05003, n=9; p <0.0001 (control *vs. Adcy5*$^{-/-}$*Adcy6*$^{-/-}$); p= 0.0017 (*Adcy5*$^{-/-}$*Adcy6*$^{-/-}$ *vs. Adcy5*$^{-/-}$ *Adcy6*$^{lox/lox}$ *MPZ*$^{cre\ -/-}$)). (**U**) CMAP duration in the same mice (control: 2.489± 0.1715, n=8; *Adcy5*$^{-/-}$*Adcy6*$^{-/-}$: 4.217± 0.3794, n=5; *Adcy5*$^{-/-}$ *Adcy6*$^{lox/lox}$ *MPZ*$^{cre+}$: 2.320± 0.1373, n=9; p <0.0001 (control *vs. Adcy5*$^{-/-}$*Adcy6*$^{-/-}$); p <0.0001 (*Adcy5*$^{-/-}$*Adcy6*$^{-/-}$ *vs. Adcy5*$^{-/-}$ *Adcy6*$^{lox/lox}$ *MPZ*$^{cre\ -/-}$)). Statistical analyses were performed using the one-way ANOVA test.

In (**B-D**), (**H-M**) and (**O-U**), bars represent the mean±SEM and each plot represents the number of mice analyzed (*n*).

Figure 5- zebrafish *adcy6a*$^{-/-}$*; adcy6b*$^{-/-}$ mutants present increased lethality, growth and behavioral impairment and defective myelin development.

(A) Schematic representation of the *adcy6a* and *adcy6b* normal and mutant alleles. The position of the mutation is indicated at the genomic level, showing a deletion of 10 nucleotides (Δ10) in *adcy6a* mutants (red) and an insertion of 29 nucleotides (+29) in *adcy6b* mutants (red). The mutation results in a frameshift leading to a premature stop codon in both alleles and truncated Adcy6a and Adcy6b proteins (*).

(B) Representative images of control *(top)* and *adcy6a*$^{-/-}$*;adcy6b*$^{-/-}$ mutant *(bottom)* adult fish showing an overall reduction in body size in mutants at 3 months.

(C) Measurement of fish length in control (2.46±0.172, n=5) and *adcy6a*$^{-/-}$*;adcy6b*$^{-/-}$**:** (1.571±0.1017, n=7; p=0.0008) at 3 months. Statistical significance was assessed using the unpaired t-test.

(D) Kaplan-Meier survival test of control (n=17) and *adcy6a*$^{-/-}$*; adcy6b*$^{-/-}$ mutants (n=22) showing a short lifespan in *adcy6a*$^{-/-}$*; adcy6b*$^{-/-}$ mutants (χi^2= 38.19, df=1 and p <0.0001). Statistical significance was assessed using the log-Rank (Mantel-Cox) test.

(E) Swimming behavior test in control (n=4) and *adcy6a*$^{-/-}$*; adcy6b*$^{-/-}$ mutants (n=4) using four categories: normal swimming (control: 100±0 and *adcy6a*$^{-/-}$*;adcy6b*$^{-/-}$**:** 0.3034±0.3034; p=0.0286), passive fall (control: 0±0 and *adcy6a*$^{-/-}$*;adcy6b*$^{-/-}$**:** 9.565±4.838; p=0.0954), discontinuous swimming (control: 0±0 and *adcy6a*$^{-/-}$*;adcy6b*$^{-/-}$**:** 50.34±12.9; p=0.0080), and immobility (control: 0±0 and *adcy6a*$^{-/-}$*; adcy6b*$^{-/-}$: 44.65±11.19; p=0.0072). The proportion of fish behavior in each category is shown. Statistical significance was assessed using the unpaired *t*-test or the Mann-Whitney test, as appropriate.

(F) Schematic image of zebrafish larvae indicating the region selected for transverse sectioning followed by representative transmission electron microscopy images of ultrathin transverse sections of the posterior lateral line nerve at 3 dpf, 4 dpf and 7 dpf in control and in *adcy6a*$^{-/-}$*; adcy6b*$^{-/-}$ mutant larvae. *(red): myelinated axon; SC: Schwann cell; a: axon. Scale bar = 0.5 μm.

(G) Number of myelinated axons per nerve at 3 dpf (control: 5.571± 0.3847, n=7; *adcy6a*$^{-/-}$*; adcy6b*$^{-/-}$**:** 0±0, n=4; p <0.0001), 4 dpf (control: 8.889± 0.3977, n=9; *adcy6a*$^{-/-}$*; adcy6b*$^{-/-}$**:** 3.167±1.093, n=3; p <0.0001) and 7 dpf (control: 12.7± 0.3, n=5; *adcy6a*$^{-/-}$*; adcy6b*$^{-/-}$**:** 7.625±0.7181, n=4; p=0.0079). Statistical significance was assessed using unpaired *t*-test or the Mann-Whitney test, as appropriate.

(H) Number of sorted axons per nerve at 3 dpf (control: 7.429± 0.6213, n=7; *adcy6a*$^{-/-}$*; adcy6b*$^{-/-}$**:** 0.75±0.75, n=4; p=0.0061), 4 dpf (control: 10.28± 0.4496, n=9; *adcy6a*$^{-/-}$*; adcy6b*$^{-/-}$**:** 7.333±0.1667, n=3; p=0.0045) and 7 dpf (control: 14.2± 0.5612, n=5; *adcy6a*$^{-/-}$*; adcy6b*$^{-/-}$**:** 11±0.9129, n=4; p=0.0167). Statistical significance was assessed using unpaired *t*-test or the Mann-Whitney test, as appropriate.

(I) Total number of axons per nerve at 3 dpf (control: 50.64± 3.141, n=7; *adcy6a*$^{-/-}$*; adcy6b*$^{-/-}$**:** 32.63±4.525, n=4; p=0.0212), 4 dpf (control: 55.67± 0.8937, n=9; *adcy6a*$^{-/-}$*; adcy6b*$^{-/-}$**:** 27.17±1.302, n=3; p<0.0001) and 7 dpf (control: 52.1± 0.8426, n=5; *adcy6a*$^{-/-}$*; adcy6b*$^{-/-}$**:** 31.88±3.217, n=4; p=0.0003). Statistical significance was assessed using unpaired *t*-test or the Mann-Whitney test, as appropriate.

(J) Percentage of myelinated axons per nerve at 3 dpf (control: 11.2± 0.928, n=7; *adcy6a*$^{-/-}$*; adcy6b*$^{-/-}$**:** 0±0, n=4; p <0.0001), 4 dpf (control: 15.93± 0.5574, n=9; *adcy6a*$^{-/-}$*; adcy6b*$^{-/-}$**:** 11.41±3.811, n=3) and 7 dpf (control: 24.38± 0.4974, n=5; *adcy6a*$^{-/-}$*; adcy6b*$^{-/-}$**:** 24.4±2.86, n=4). Statistical significance was assessed using unpaired *t*-test.

(K) Percentage of axons per diameter in 3 dpf zebrafish larvae with 0.1 μm bin width : 0-0.1 μm, 0.1-0.2 μm, 0.2-0.3 μm, 0.3-0.4 μm, 0.4-0.5 μm, 0.5-0.6 μm, 0.6-0.7 μm, 0.7-0.8 μm, 0.8-

0.9 μm, 0.9-1 μm and over 1 μm (1+). A significative difference was observed in very small caliber axons (0.1-0.2) μm axons ($p < 0.0001$). Statistical analyses were performed using the two-way ANOVA test.

(**L**) Representative confocal microscopy images of the posterior lateral line within a defined region showing Schwann cells labeled in green (anti-GFP) and the proliferating cells labelled in red (anti-PH3) in control *foxd3:gfp* and *adcy6a*$^{-/-}$*; adcy6b*$^{-/-}$*foxd3:gfp* mutant embryos at 48hpf. Scale bar = 20 μm.

(M) Total number of Schwann cells within a defined region of the PLLn in control and in *adcy6a*$^{-/-}$*; adcy6b*$^{-/-}$ mutant embryos at 48hpf (control: 67.12$\pm$ 2.658, n=17; *adcy6a*$^{-/-}$*; adcy6b*$^{-/-}$: 70.67$\pm$2.877, n=12, p=0.3809) and 72 hpf (control: 75.2$\pm$ 2.533, n=10; *adcy6a*$^{-/-}$*; adcy6b*$^{-/-}$: 76.86$\pm$ 3.45, n=14, p=0.7234). Statistical significance was assessed using the unpaired t-test.

(N) Proliferating Schwann cells at 48hpf (control: 1.864$\pm$ 0.3797, n=22; *adcy6a*$^{-/-}$*; adcy6b*$^{-/-}$: 1.75$\pm$ 0.4787, n=12) and 72 hpf (control: 1.5$\pm$ 0.5, n=10; *adcy6a*$^{-/-}$*; adcy6b*$^{-/-}$: 0.9286$\pm$ 0.2215, n=14). Statistical significance was assessed using the unpaired *t*-test or the Mann-Whitney test, as appropriate.

In (**C-E**), **(G-K)** and (**M,N**), bars represent the mean$\pm$SEM and each plot represents the number of fish/larvae analyzed (*n*).

Figure 6- Adcy6 is the key driver of Gpr126 early myelin activity mainly via GPR126-cAMP-PKA signaling pathway

(A) Schematic representation of the signaling pathway and pharmacological treatments used in this experiment.

(B) Representative *in situ* hybridization images showing the four *mbp* expression levels in zebrafish larvae at 3dpf scored in these experiments: normal expression, some expression, weak expression and no expression.

(C) and **(D)** Percentage of the different *mbp* expression levels in larvae across different experimental groups: WT (n=80), WT + FSK (n=17), WT + 8-CPT-cAMP (n=12), WT + 6-Bnz-cAMP (n=20), MO *gpr126* (n=58), MO *gpr126* + FSK (n=31), MO *gpr126* + *adcy6a*$^{-/-}$*; adcy6b*$^{-/-}$ (n=17), MO *gpr126* + *adcy6a*$^{-/-}$*; adcy6b*$^{-/-}$ +FSK (n=12), *adcy6a*$^{-/-}$*; adcy6b*$^{-/-}$ (n=22), *adcy6a*$^{-/-}$*; adcy6b*$^{-/-}$ + FSK (n=16), *adcy6a*$^{-/-}$*; adcy6b*$^{-/-}$ + 8-CPT-cAMP (n=11), *adcy6a*$^{-/-}$*; adcy6b*$^{-/-}$ + 6-Bnz-cAMP (n=16), *adcy6a*$^{-/-}$*; adcy6b*$^{-/-}$ + *psox10:actPKA* (n=13), *adcy6a*$^{-/-}$*; adcy6b*$^{-/-}$ + *psox10:GFP* (n=5). **(C)** WT *vs.* MO *gpr126* ($p < 0.0001$), WT *vs. adcy6a*$^{-/-}$*; adcy6b*$^{-/-}$ ($p < 0.0001$), MO *gpr126 vs.* MO *gpr126* + FSK (<0.0001), MO *gpr126* + FSK *vs.* MO *gpr126*

+ *adcy6a*$^{-/-}$*; adcy6b*$^{-/-}$ +FSK (p <0.0001) and *adcy6a*$^{-/-}$*; adcy6b*$^{-/-}$ *vs. adcy6a*$^{-/-}$*; adcy6b*$^{-/-}$ + 6-Bnz-cAMP (p= 0.0002). **(D)** WT *vs. adcy6a*$^{-/-}$*; adcy6b*$^{-/-}$ (p <0.0001), WT *vs. adcy6a*$^{-/-}$*; adcy6b*$^{-/-}$ + *psox10:actPKA* (p <0.0001), WT *vs. adcy6a*$^{-/-}$*; adcy6b*$^{-/-}$ + *psox10:GFP* (p <0.0001), *adcy6a*$^{-/-}$*; adcy6b*$^{-/-}$ *vs. adcy6a*$^{-/-}$*; adcy6b*$^{-/-}$ + *psox10:actPKA* (p <0.0001), *adcy6a*$^{-/-}$*; adcy6b*$^{-/-}$ + *psox10:actPKA vs. adcy6a*$^{-/-}$*; adcy6b*$^{-/-}$ + *psox10:GFP* (p <0.0001). Statistical analyses were performed using the Fischer's exact test.

Figure 7- *adcy6* mutants present reduced neuronal numbers in the PLLg and impaired axonal mitochondrial transport.

(A) Representative confocal images of the posterior lateral line ganglion (PLLg) in control and *adcy6a*$^{-/-}$*; adcy6b*$^{-/-}$ larvae at 48hpf. Neuronal cells are labeled in red (anti-HUC). Scale bar = 10 μm.

(B) Number of neurons within the PLLg at 48hpf (control: 59.27± 0.9658, n=10; *adcy6a*$^{-/-}$*; adcy6b*$^{-/-}$: 41.47± 1.706, n=10; p <0.0001) and at 72hpf (control: 70.96± 2.774, n=9; *adcy6a*$^{-/-}$*; adcy6b*$^{-/-}$: 56.75± 2.125, n=8; p= 0.0012). Statistical analysis was performed using unpaired t-test.

(C) Representative confocal images of the posterior lateral line nerve (PLLn) showing axonal growth in control and *adcy6a*$^{-/-}$*; adcy6b*$^{-/-}$ larvae at 48hpf. The PLLn is labeled in red (anti-Actub). Scale bar = 100 μm.

(D) Axonal growth of the PLLn at 48hpf relative to full body length (control: 90.14± 1.03, n=10; *adcy6a*$^{-/-}$*; adcy6b*$^{-/-}$: 89.71± 1.155, n=11) showing no significative difference between control and mutant embryos. Statistical significance was assessed using unpaired t-test.

(E) Representative confocal microscopy images showing the anterograde (white arrows) and retrograde (red arrows) transport of mitochondria (labelled in green with mito-GFP) in the PLLn axons of control and *adcy6a*$^{-/-}$*; adcy6b*$^{-/-}$ larvae at 48hpf. Scale bar=10 μm.

(F) Axonal transport analysis in control and *adcy6a*$^{-/-}$*; adcy6b*$^{-/-}$ larvae at 48 hpf showing a significant decrease in mitochondrial anterograde speed (control: 1.001± 0.04537, n=11; *adcy6a*$^{-/-}$*; adcy6b*$^{-/-}$: 0.7799± 0.02788, n=7; p= 0.0024), retrograde speed (control: 1.708± 0.097, n=11; *adcy6a*$^{-/-}$*; adcy6b*$^{-/-}$*:* 0.9072± 0.08411, n=6; p <0.0001) and flux density (control: 2.549± 0.2332, n=9; *adcy6a*$^{-/-}$*; adcy6b*$^{-/-}$: 1.197± 0.09362, n=7; p= 0.0003). Statistical significance was assessed using unpaired t-test.

In (**B**), **(D)** and (**E**), bars represent the mean±SEM and each plot represents the number of larvae analyzed (*n*).

Figure 8- *adcy6* mutants display defects in sodium channel clustering at nodes of Ranvier.
(A) Representative confocal microscopy images showing Nach clustering at nodes of Ranvier in green (anti-NaCh) within a defined region along the axons of the PLLn labeled in red (anti-Actub) and their respective merge stills in WT and *adcy6a*$^{-/-}$*; adcy6b*$^{-/-}$ larvae at 4dpf. Scale bar= 5 μm.
(B) Number of NaCh clusters within a defined region in the anterior part of the PLLn (control: 4.864± 0.2344, n=11; *adcy6a*$^{-/-}$*; adcy6b*$^{-/-}$: 3.389± 0.2469, n=9; p= 0.0004) and within a defined region in the posterior part (control: 4.818± 0.3521, n=11; *adcy6a*$^{-/-}$*; adcy6b*$^{-/-}$: 2.111± 0.1111, n=9; p<0.0001). Statistical analyses were performed using an unpaired *t*-test or the Mann-Whitney test, as appropriate.
(C) Number of NaCh clusters within a defined region in WT (anterior region: 4.864± 0.2344, n=11; posterior region: 5.000± 0.4629, n=8; p<0.0001) and in *adcy6a*$^{-/-}$*;adcy6b*$^{-/-}$ mutant embryos (anterior region: 3.389± 0.2469, n=9; Posterior region: 2.111± 0.1111, n=9; p= 0.0015) larvae. Statistical analyses were performed using an unpaired *t*-test or the Mann-Whitney test, as appropriate.
(D) Ratio Anterior/Posterior of NaCh clusters in WT (1.055±0.08094, n=11) and *adcy6a*$^{-/-}$*; adcy6b*$^{-/-}$ **(**1.630±0.1362, n=9, p=0.0014) larvae. Statistical analysis was performed using unpaired t-test.
(E) Representative confocal microscopy images showing Nach clustering at nodes of Ranvier in green (anti-NaCh) along the axons of the PLLn labeled in red (anti-Actub) and their respective merge stills in *adcy6a/b* morphants (top panel) at 4dpf. Scale bar= 5 μm. NaCh clustering is observed in WT axons (mCherry red labeled) while surrounding *adcy6a/b* morphant axons present little or no NaCh clustering (middle panel) in chimeric PLL neurons. NaCh clustering is absent in *adcy6a/b* morphant axons (mCherry red labeled) while adjacent WT axons in the same PLLn show normal clustering (bottom panel). Scale bar= 5 μm.
(F) Number of NaCh clusters in WT (9.5±0.7188, n=6) and *adcy6a/b* morphant (1.333±0.4944, n=6, p<0.0001) larvae. Statistical analysis was performed using unpaired t-test.
In (**B-E**), bars represent the mean±SEM and each plot represents the number of larvae analyzed (*n*).

Materials and methods

Animal models

Mice strains

C57BL/6J mice at different stages were used in this study. Knockout (KO) mice for *Adcy5* (*Adcy5*$^{-/-}$) and KO mice for *Adcy6* (*Adcy6*$^{-/-}$) were kindly provided by university of Oslo and crossed to obtain double knockout mice *Adcy5*$^{-/-}$/*Adcy6*$^{-/-}$. *Adcy6* conditional knockout mice (*Adcy6*$^{lox/lox}$ *MPZ*$^{cre+}$ or cKO) were generated using Cre-Lox system. *Adcy6* homozygous for lox mice, *Adcy6*$^{lox/lox}$ (strain no. 022503, the Jackson Laboratory) were crossed with MPZ-cre line (strain no. 017927, the Jackson Laboratory), which express Cre recombinase specifically in Schwann cells from E12. This strain was crossed with *Adcy5*$^{-/-}$ mice to generate the *Adcy5*$^{-/-}$ *Adcy6*$^{lox/lox}$ *MPZ*$^{cre+}$ mice. Tail biopsies were used to perform DNA extraction using Direct PCR (no. 102-T, VIAGEN) and Proteinase K (no. BP1700-100, Fisher bioreagents). PCR-RFLP (Restriction Fragment Length Polymorphism) with specific primers to each gene were used to identify mice (Supplementary 1).

Animals were maintained under standard laboratory conditions (license number: G 9404313 and specific animal authorizations: #13832-2018022616275493 v3 and #26850-202007291424987 v2), including controlled temperature (20°C to 24°C), humidity (55±10%) and a 12h light/dark cycle. Mice were housed in groups, with a maximum of five animals per cage, with ad libitum access to water.

Zebrafish strains

Embryo care

Danio rerio fish and embryos (AB strain) were used in this study. Embryos were staged and cared for according to standard protocols (https://zfin.org/zf_info/zfbook/cont.html) and all zebrafish were maintained under standard conditions at the Kremlin Bicêtre zebrafish facility. Adult animals were kept in a 14 hours and 10 hours light cycle. *Tg(foxd3:gfp)* stable transgenic line was used to label SCs[59]. Embryos were kept at 29ºC in egg water with methylene blue or embryo medium. All experiments were performed on larvae up to 7dpf. All animal experiments were conducted with approved protocols at Inserm by DDPP Val de Marne, France under license number G 9404313.

adcy6a and *adcy6b* CRISPR mutagenesis

sgRNA sequence GCTCCCCGCAGTGCCTCGGAGGG targeting adcy6a exon 3 and sgRNA sequence GAAGCGTACGCCACATCTGGGGG targeting adcy6b exon 3 were designed using CRISPOR program (www.crsipror.tefor.net). In vitro transcription of the sgRNAs was performed using the HiScribe T7 Quick High Yield RNA synthesis kit (New England Biolabs) and sgRNAs were purified using ZYMO Clean&Concentrator-5 kit (Ozyme).

To generate *adcy6a* mutants, 100 ng/µl of sgRNA was injected into one-cell stage embryos with Cas9 endonuclease (NEB M0386M; final concentration 20 µM). The loss of function mutant showing a deletion of 10 nucleotides in *adcy6a* was used in this study. A restriction enzyme cut-site was generated and was used to identify the mutation and distinguish WT from mutants (Supplementary 2 and 3). The same strategy was used to generate *adcy6b* mutants. The loss of function mutation showing a 29-nucleotide insertion was used in this study.

Animal studies

Microinjections

psox10:PKA^{act} (kindly provided by William Talbot) and *psox10:EGFP* were injected separately or in combination at 20 pg per zebrafish embryo along with 100 pg of Tol2 transposase mRNA. Synthetic mRNA of *mito:GFP* and *mCherry* were prepared using SP6 mMessage mMachine System (no. EP0131, Thermo Fisher Scientific) after linearization with Not1 (no. R3189L, NEB) and injected at 100 pg per embryo.

To significantly reduce Gpr126 activity, zebrafish embryos were injected at one cell stage with 15 ng of *gpr126* morpholino (5'-ACAGAATATGAATACCTGATACTCC-3'). 0.3 mM of each of the two *adcy6a* and *adcy6b* MO were mixed (final concentration: 0.6 mM) and injected (v=1 nl/embryo) into one to four cell-stage embryos to significantly deplete *adcy6a and b* function in embryos.

In situ hybridization

Different groups of depigmented (PTU-treated) control and *adcy6* mutant zebrafish embryos were used to detect *mbp* RNA expression in whole-mount in situ hybridization. The *mbp* RNA probe was synthesized using the SP6 polymerase following linearization with EcoRI (no. R601A, Promega) and using the DIG RNA labeling kit. Embryos were fixed at 72hpf in 4% paraformaldehyde (PFA) prepared in 1XPBS overnight at 4°C. They were then washed in a 1:1 mixture of 1XPBS and 100% MeOH (1:1) and transferred to 100% MeOH for storage at -20°C. Prior to hybridization, embryos were rehydrated through a graded PBSTw (1XPBS containing 0.1% Tween-20)-100% MeOH series: 1 x 5 minutes 50%PBSTw-50%MeOH100%, 1 x 5

minutes 70%PBSTw-30%MeOH100% followed by 4 x 5 minutes PBSTw. Embryos were permeabilized with Proteinase K (10mg/ml, diluted 1:500 in 1XPBS) for 45 minutes, rinsed with PBSTw, and post-fixed in 4% PFA (in 1XPBS) for 20 minutes at room temperature. After extensive washing with PBSTw, embryos were prehybridized in hybridization buffer (HB) for a minimum of 2 hours at 65°C, then hybridized overnight at the same temperature with 180 ng of probe in 200 µl of HB (Supplementary 4). The following day, embryos underwent six different post-hybridization washes in HB/SSCTw at 65°C to remove unbound probe. After washing in PBSTw, embryos were blocked in blocking solution for at least 2 hours at room temperature and then incubated overnight at 4°C with an anti-digoxygenin antibody (no. 11093274910, Roche) diluted at 1:2000 in blocking solution. On the next day, embryos were washed 6 times for 30 minutes in PBSTw at room temperature and then left in PBSTw overnight at 4°C. Embryos were incubated in freshly prepared alkaline phosphatase (AP) buffer for 10 minutes, followed by incubation in AP buffer containing NBT-BCIP mix (100 µl NBT-BCIP mix in 5ml AP Buffer; no. 11681451001, Roche) for 3 hours in the dark at room temperature, until the desired signal intensity was reached. The color reaction was stopped by rinsing embryos several times with water. Embryos were then imaged under a microscope and categorized into four levels of expression of *mbp*: Normal, Some, Low and No expression. All solutions used in this experiment are listed in the supplementary materials (Supplementary 4).

Immunostaining

The following antibodies and dilutions were used: mouse anti-acetylated tubulin (Sigma; 1/500; T7451), rabbit anti-phospho Histone 3 (Ser 10) (Millipore; 1/500; Cat # 06-570), mouse anti-sodium channels (pan) clone K38/35 (Sigma; 1/500), chicken anti-EGFP (Abcam; 1/500; AB13970), mouse anti HuC (Invitrogen, 1/500; A21271). Primary antibodies were detected with appropriate secondary antibodies conjugated to either Alexa 488, Alexa 568 at a 1:500 dilution (Supplementary 5). For immunostaining, zebrafish embryos were fixed in 4% paraformaldehyde 1X PBS overnight at 4°C, then dehydrated in methanol at -20°C. Samples were then rehydrated, digested with proteinase K and blocked with 0.5% triton in PBS and 10% sheep serum and then incubated with primary antibody overnight at 4°C (diluted in PBS+2% sheep serum). Larvae were then washed with PBS for a few hours and then incubated with secondary antibody in 0.5% triton in PBS and 2% sheep serum overnight at 4°C. For NaCh/acetylated tubulin staining, embryos were fixed in 4% PFA for 30 min and treated for 7 min with acetone at -20°C. Samples were then blocked with 0.5% triton in PBS and 10% sheep

serum and then incubated with primary antibody overnight at 4°C (diluted in PBS+2% sheep serum). Larvae were then washed with PBS for a few hours and then incubated with secondary antibody in 0.5% triton in PBS and 2% sheep serum for 3 hours at RT. Embryos were then washed and then mounted to be imaged using a Leica SP8 confocal microscope.

Pharmacological treatment

Zebrafish embryos were incubated in fish water containing compounds diluted in DMSO. The following compounds and procedures were used: Forskolin (Selleckchem, S2449) 20 μM at 48 hpf for 3 hours; 6-Bnz-cAMP (BIOLOG, B009), 1 mM, from 48 hpf until 72 hpf; 8-CPT-cAMP (BIOLOG, C010), 1 mM, from 48 hpf until 72 hpf.

Controls were incubated in equivalent amount of DMSO solution (0.1%) during the same period.

Acridine orange staining

Zebrafish embryos were anesthetized with 0.03% tricaine and incubated in fish water containing 5 μM acridine orange for 20 minutes in the dark. Embryos were washed, embedded in 1.5% low melting point agarose, and imaged with a Leica SP8 confocal microscope. Transmitted light imaging was used to identify the PLLg.

Schwann cells, PH3 positive SCs and neuronal HuC positive counts

Control *Tg(foxd3:gfp)* and *adcy6a*$^{-/-}$*;adcy6b*$^{-/-}$*/ Tg(foxd3:gfp)* zebrafish embryos were imaged using Leica SP8 confocal microscope. SCs and PH3 positive SCs were counted from the most anterior to the end of yolk extension along the AP axis (≈900 μm) following immunostaining and using image J. Total neuronal HuC positive cells in WT and *adcy6a*$^{-/-}$*;adcy6b*$^{-/-}$ embryos were counted from confocal z-series of the whole PLLg following HuC immunostaining, using image J. Cells were counted blindly by two independent researchers.

Live imaging

WT and *adcy6a*$^{-/-}$*;adcy6b*$^{-/-}$ zebrafish embryos were anesthetized with 0.03% tricaine and embedded in 1.5% low melting point agarose. Recordings of *mito:gfp* within the PLLn were performed at 27°C using a Leica SP8 confocal microscope. Embryos were examined at 48hpf and imaged from a lateral view with a series of 10 min time-lapses. Movies were then cropped and assembled at a speed of 7 frames/second and saved as QuickTime movie files.

Chimeric analysis

adcy6a/b MOs (0.6 pmoles) and mCherry mRNA (200ng/µl) were injected into donor zebrafish embryos. Morphant/fluorescent cells were then introduced into a WT background. mCherry WT cells were also established within *adcy6a/b* MOs background. Embryos showing mCherry labeling within the PLLg/PLLn were selected for sodium channel clustering immunostaining and analysis.

Transmission Electron microscopy and optical microscopy of peripheral nerves

Sciatic nerves from controls and mutant mice at P5, P10 and adult stages were dissected and fixed overnight at 4°C with Solution 1 (Supplementary 6). Zebrafish embryos at 3dpf, 4dpf and 7dpf were transversely sectioned through the trunk just posterior to the yolk using a fine scalpel. The posterior segment containing the posterior lateral line nerve (PLLn) was fixed overnight at 4°C in Solution 2, while the anterior segment containing the head was used for DNA extraction followed by PCR-RFLP to identify the mutant embryos. Following fixation, samples were washed with 0.1M sodium cacodylate buffer (no. 12310, Electron Microscopy Sciences) and post-fixed for 50 minutes at 4°C with osmium tetroxide diluted in 0.1M sodium cacodylate buffer (2% for zebrafish embryos and 1% for sciatic nerve, no. 19152, Electron Microscopy Sciences). After rinsing in distilled water, samples were incubated in 2% uranyl acetate at room temperature to enhance contrast. Samples were then dehydrated through a graded ethanol series (40%, 60%, 80% and 100%), with two washes of 10 minutes at each concentration, followed by a brief incubation in acetone for 2 minutes. Tissues were then put in a mix of 1:1 epoxy resin and acetone for 15 minutes at room temperature, then transferred to pure epoxy resin (Supplementary 6) and incubated overnight at 4°C. The following day, samples were degassed for 3 hours, embedded in molds to allow transverse sectioning and polymerized at 65°C for 48 hours.

Ultrathin sections of 0.4 um were prepared using ultramicrotome and collected in a single-slot grids coated with a support film. Sections were examined using a transmission electron microscope (JEOL, JEM1400). For mouse sciatic nerves, images were acquired at a field size of 570 um (except adult cKO), with ten fields analyzed per nerve. For zebrafish PLLn samples, the entire nerve was imaged.

Semi-thin sections of 1 um were cut using an ultramicrotome, treated with sodium hydroxide for 20 minutes to remove resin, rinsed through three baths of 100% ethanol followed by one water bath, and stained with toluidine blue for 1 hour at 62°C. Sections was then dehydrated

through three baths of 100% ethanol, cleared in three baths of xylene and mounted on glass slides.

Images were analyzed using ImageJ software. The number of axons was quantified using the "cell counter" tool, and axonal diameter and area were measured using the "straight line" and "freehand" respectively followed by the "measure" tool.

Functional tests

Pole test

The Pole test consists of a vertical wooden pole (50 cm in length and 8 mm in diameter) mounted on a horizontal support. Mice are placed at the top of the pole, facing downward. Performance was evaluated using a binary scoring system. Animals that descended the pole normally using their four limbs and without impairment were assigned a score of 1. In contrast, mice exhibiting motor deficits, including hindlimb impairment, sliding or falling were assigned a score of 0.

Tail suspension test

The tail suspension test was performed to evaluate limb clasping behavior in mice. Animals were individually suspended by the tail and maintained in suspension for 3 minutes. During this period, the position and movement of the forelimbs and hindlimbs were carefully observed. Limb clasping was analyzed and scored using a five-point scale (0 to 4) based on the severity of the paw contraction: score 0, no limb clasping; score 1, one hindlimb exhibits incomplete splay and loss of mobility and toes exhibit normal splay; score 2, two hindlimbs exhibit incomplete splay and loss of mobility and toes exhibit normal splay; score 3, both hindlimbs exhibit clasping with curled toes and immobility; score 4, forelimbs and hindlimbs exhibit clasping and are crossed with curled toes and immobility. Final results were expressed as the percentage of animals exhibiting limb clasping defects at each score.

Electrophysiological measurements

The experiment was performed using an EMG LT Surpass Amplifier machine (EMS Biomedical, Korneuburg, Austria). Anesthesia in two-months-mice was induced with 5% isoflurane and maintained at 2% throughout the procedure. Body temperature was maintained at 37℃ using a thermostatically controlled heating pad. Mice were positioned in prone position, and the hindlimbs were gently extended. Hindlimb compound motor action potentials (CMAPs) were recorded using needle electrodes. Stimulating electrodes were placed along the sciatic nerve at the level of the spinal ganglion, with an interelectrode distance of approximately

2 cm. The recording electrode was inserted into the gastrocnemius muscle and the reference electrode was placed on the tail of the mouse. The ground electrode was positioned on the contralateral hindlimb. Recordings were performed at a stimulation intensity of 8 mA.

RNA isolation and RT-qPCR

Total RNA was isolated from sciatic nerves of mice at different stages, as well as from brain and embryonic DRG using TRIzol® Reagent (no. 15596018, ambion) followed by RNA purification performed using RNeasy Mini kit (no. 217004, Qiagen, France) according to manufacturer's instructions. RNA concentration was determined using NanoDrop® ND-1000 spectrophotometer. A minimum of 50 ng total RNA was reverse transcribed using High Capacity cDNA Reverse Transcription Kit (no. 4368814, Applied Biosystems, UK), following manufacturer's instructions.

qPCR was performed in a 20µl reaction mix containing 10 µl of Applied Biosystems PowerSYBR® GREEN PCR Master Mix (no. 4367659, Thermo Fisher Scientific), 0.1 µl of 100 µM primers or 0.2 µl of 50 µM primers (Supplementary 7), and 2 µl of cDNA, using the 7300 system program. Quantification was performed using the $2^{-\Delta CT}$ method for gene expression analysis and $2^{-\Delta\Delta CT}$ method for gene expression in mutants relative to WT (set to 1). Target gene expression was normalized to cyclophilin A (cycloA) mRNA and expressed relative to the control condition, which was set to 1.

Statistical analysis

Means and standard deviations were calculated with Graph Pad Prism 10. All data were first tested for normal distribution using the Shapiro–Wilk normality test combined with D'Agostino & Pearson normality test. All experiments with only two groups and one dependent variable were compared using an unpaired *t*-test if they passed normality test; if not, groups were compared with the nonparametric Mann-Whitney test. Statistically significant differences were determined using one-way ANOVA test for all experiments with more than two groups but only one dependent variable if data were normally distributed; if not, groups were compared using Kruskal-Wallis test. Two-way ANOVA test was used for all experiments with more than two groups and two dependent variables. Error bars depict standard errors of the mean (SEM). ns, $p > 0.05$; *, $p \leq 0.05$; **, $p \leq 0.01$; ***, $p \leq 0.001$; ****, $p \leq 0.0001$.

Acknowledgments

We thank TEM facility of Imagerie-Gif (I2BC) supported by ANR-24-INBS-0005 (BIOGEN); ANR-17-EUR-0007, EUR SPS-GSR); ITMO Cancer of Aviesan and INCa, Julien Loisel-Duwattez, Luc Bousset, Chie Kodera and Xavier Heiligenstein (CryoCapCell) for technical help in TEM, William Talbot for *psox10:PKA^{act}* construct, Kurt Allen Krobet and Finn Olav Levy (Oslo University Hospital, Norway) for *Adcy5* and *Adcy6* KO mice. This work was funded by AFM (Grant 23097) to M.T., Inserm and University Paris-Saclay.

Declarations

Funding

This work was supported by AFM (Grant number 23097) to M.T and by University Paris Saclay and Inserm.

Competing interests

The authors have no relevant financial or non-financial interests to disclose.

Author contribution

M.T. conceived and funded the project. M.T., O.H., and MJ.B. designed the experiments. O.H., MJ.B., F.M., A.-E.L., F.M., and M.T. performed the experiments. J.M. and A.-E.L. provided expertise. O.H. and M.T. wrote the manuscript.

Data availability

The datasets generated during the current study are available from the corresponding author upon request.

Ethics approval

This study was performed in line with the principles of the Declaration of Helsinki. Approval is granted by the Ethics committee of DDPP Val de Marne, France under license number G 9404313.

Consent to participate and to publish

N.A

References

1. Jessen, K. R. & Mirsky, R. The origin and development of glial cells in peripheral nerves. *Nat. Rev. Neurosci.* **6**, 671–682 (2005).
2. Woodhoo, A. & Sommer, L. Development of the Schwann cell lineage: from the neural crest to the myelinated nerve. *Glia* **56**, 1481–1490 (2008).
3. Jessen, K. R. & Mirsky, R. Schwann Cell Precursors; Multipotent Glial Cells in Embryonic Nerves. *Front. Mol. Neurosci.* **12**, 69 (2019).
4. Zalc, B. The acquisition of myelin: An evolutionary perspective. *Brain Res.* **1641**, 4–10 (2016).
5. Waxman, S. G. Determinants of conduction velocity in myelinated nerve fibers. *Muscle Nerve* **3**, 141–150 (1980).
6. Hartline, D. K. & Colman, D. R. Rapid Conduction and the Evolution of Giant Axons and Myelinated Fibers. *Curr. Biol.* **17**, R29–R35 (2007).
7. Appenzeller, O. & Palmer, G. The cyclic AMP (adenosine 3′,5′-phosphate) content of sciatic nerve: changes after nerve crush. *Brain Res.* **42**, 521–524 (1972).
8. Sobue, G., Shuman, S. & Pleasure, D. Schwann cell responses to cyclic AMP: proliferation, change in shape, and appearance of surface galactocerebroside. *Brain Res.* **362**, 23–32 (1986).
9. Morgan, L., Jessen, K. R. & Mirsky, R. The effects of cAMP on differentiation of cultured Schwann cells: progression from an early phenotype (04+) to a myelin phenotype (P0+, GFAP-, N-CAM-, NGF-receptor-) depends on growth inhibition. *J. Cell Biol.* **112**, 457–467 (1991).
10. Arthur-Farraj, P. *et al.* Mouse schwann cells need both NRG1 and cyclic AMP to myelinate. *Glia* **59**, 720–733 (2011).

11. Bacallao, K. & Monje, P. V. Opposing Roles of pka and epac in the cAMP-Dependent Regulation of Schwann Cell Proliferation and Differentiation. *PLoS ONE* **8**, e82354 (2013).
12. Monk, K. R. *et al.* A G Protein–Coupled Receptor Is Essential for Schwann Cells to Initiate Myelination. *Science* **325**, 1402–1405 (2009).
13. Monk, K. R., Oshima, K., Jörs, S., Heller, S. & Talbot, W. S. Gpr126 is essential for peripheral nerve development and myelination in mammals. *Development* **138**, 2673–2680 (2011).
14. Mogha, A. *et al.* Gpr126 Functions in Schwann Cells to Control Differentiation and Myelination via G-Protein Activation. *J. Neurosci.* **33**, 17976–17985 (2013).
15. Laquerriere, A. *et al.* Mutations in CNTNAP1 and ADCY6 are responsible for severe arthrogryposis multiplex congenita with axoglial defects. *Hum. Mol. Genet.* **23**, 2279–2289 (2014).
16. Khannpnavar, B., Mehta, V., Qi, C. & Korkhov, V. Structure and function of adenylyl cyclases, key enzymes in cellular signaling. *Curr. Opin. Struct. Biol.* **63**, 34–41 (2020).
17. Ravenscroft, G. *et al.* Mutations of GPR126 Are Responsible for Severe Arthrogryposis Multiplex Congenita. *Am. J. Hum. Genet.* **96**, 955–961 (2015).
18. Petersen, S. C. *et al.* The Adhesion GPCR GPR126 Has Distinct, Domain-Dependent Functions in Schwann Cell Development Mediated by Interaction with Laminin-211. *Neuron* **85**, 755–769 (2015).
19. Halls, M. L. & Cooper, D. M. F. Adenylyl cyclase signalling complexes – Pharmacological challenges and opportunities. *Pharmacol. Ther.* **172**, 171–180 (2017).
20. Gerber, D. *et al.* Transcriptional profiling of mouse peripheral nerves to the single-cell level to build a sciatic nerve ATlas (SNAT). *eLife* **10**, e58591 (2021).

21. Tang, T. *et al.* Adenylyl Cyclase Type 6 Deletion Decreases Left Ventricular Function via Impaired Calcium Handling. *Circulation* **117**, 61–69 (2008).
22. Cosson, M.-V., Hiis, H. G., Moltzau, L. R., Levy, F. O. & Krobert, K. A. Knockout of adenylyl cyclase isoform 5 or 6 differentially modifies the β1-adrenoceptor-mediated inotropic response. *J. Mol. Cell. Cardiol.* **131**, 132–145 (2019).
23. Lee, K.-W. *et al.* Impaired D2 dopamine receptor function in mice lacking type 5 adenylyl cyclase. *J. Neurosci. Off. J. Soc. Neurosci.* **22**, 7931–7940 (2002).
24. Phan, H. M., Gao, M. H., Lai, N. C., Tang, T. & Hammond, H. K. New signaling pathways associated with increased cardiac adenylyl cyclase 6 expression: implications for possible congestive heart failure therapy. *Trends Cardiovasc. Med.* **17**, 215–221 (2007).
25. Chen-Goodspeed, M., Lukan, A. N. & Dessauer, C. W. Modeling of Galpha(s) and Galpha(i) regulation of human type V and VI adenylyl cyclase. *J. Biol. Chem.* **280**, 1808–1816 (2005).
26. Hwang, W. Y. *et al.* Efficient genome editing in zebrafish using a CRISPR-Cas system. *Nat. Biotechnol.* **31**, 227–229 (2013).
27. Mikdache, A. *et al.* Timely Schwann cell division drives peripheral myelination *in vivo* via the laminin/cAMP pathway. *Development* **149**, dev200640 (2022).
28. Cunningham, R. L. & Monk, K. R. Live Imaging of Schwann Cell Development in Zebrafish. *Methods Mol. Biol.* **1739**, 401–405 (2018).
29. Boueid, M.-J., Mikdache, A., Lesport, E., Degerny, C. & Tawk, M. Rho GTPases Signaling in Zebrafish Development and Disease. *Cells* **9**, 2634 (2020).
30. Glenn, T. D. & Talbot, W. S. Analysis of Gpr126 function defines distinct mechanisms controlling the initiation and maturation of myelin. *Development* **140**, 3167–3175 (2013).

31. El-Hage, O., Mikdache, A., Boueid, M.-J., Degerny, C. & Tawk, M. Schwann cells have a limited window of time in which to initiate myelination signaling during early migration in vivo. *Cells Dev.* **181**, 203993 (2025).
32. Carney, T. J. *et al.* A direct role for Sox10 in specification of neural crest-derived sensory neurons. *Development* **133**, 4619–4630 (2006).
33. Vagnoni, A. & Bullock, S. L. A cAMP/PKA/Kinesin-1 Axis Promotes the Axonal Transport of Mitochondria in Aging Drosophila Neurons. *Curr. Biol.* **28**, 1265-1272.e4 (2018).
34. Zhang, Y. *et al.* Assembly and Maintenance of Nodes of Ranvier Rely on Distinct Sources of Proteins and Targeting Mechanisms. *Neuron* **73**, 92–107 (2012).
35. Mokuno, K. *et al.* Regulation of Schwann cell nerve growth factor receptor by cyclic adenosine 3',5'-monophosphate. *J. Neurosci. Res.* **21**, 465–472 (1988).
36. Monje, P. V. To myelinate or not to myelinate: fine tuning cAMP signaling in Schwann cells to balance cell proliferation and differentiation. *Neural Regen. Res.* **10**, 1936–1937 (2015).
37. Laquerriere, A. *et al.* Phenotypic spectrum and genomics of undiagnosed arthrogryposis multiplex congenita. *J. Med. Genet.* **59**, 559–567 (2022).
38. Otte, A. P., Van Run, P., Heideveld, M., Van Driel, R. & Durston, A. J. Neural induction is mediated by cross-talk between the protein kinase C and cyclic AMP pathways. *Cell* **58**, 641–648 (1989).
39. Vossler, M. R. *et al.* cAMP activates MAP kinase and Elk-1 through a B-Raf- and Rap1-dependent pathway. *Cell* **89**, 73–82 (1997).
40. Lipskaia, L., Djiane, A., Defer, N. & Hanoune, J. Different expression of adenylyl cyclase isoforms after retinoic acid induction of P19 teratocarcinoma cells. *FEBS Lett.* **415**, 275–280 (1997).

41. Lepski, G., Jannes, C. E., Nikkhah, G. & Bischofberger, J. cAMP promotes the differentiation of neural progenitor cells in vitro via modulation of voltage-gated calcium channels. *Front. Cell. Neurosci.* **7**, 155 (2013).
42. Perge, J. A., Niven, J. E., Mugnaini, E., Balasubramanian, V. & Sterling, P. Why do axons differ in caliber? *J. Neurosci. Off. J. Soc. Neurosci.* **32**, 626–638 (2012).
43. Leterrier, C., Dubey, P. & Roy, S. The nano-architecture of the axonal cytoskeleton. *Nat. Rev. Neurosci.* **18**, 713–726 (2017).
44. Nixon, R. A., Paskevich, P. A., Sihag, R. K. & Thayer, C. Y. Phosphorylation on carboxyl terminus domains of neurofilament proteins in retinal ganglion cell neurons in vivo: influences on regional neurofilament accumulation, interneurofilament spacing, and axon caliber. *J. Cell Biol.* **126**, 1031–1046 (1994).
45. Costa, A. R., Pinto-Costa, R., Sousa, S. C. & Sousa, M. M. The Regulation of Axon Diameter: From Axonal Circumferential Contractility to Activity-Dependent Axon Swelling. *Front. Mol. Neurosci.* **11**, 319 (2018).
46. Pelletier, S., Julien, C., Popoff, M. R., Lamarche-Vane, N. & Meloche, S. Cyclic AMP induces morphological changes of vascular smooth muscle cells by inhibiting a Rac-dependent signaling pathway. *J. Cell. Physiol.* **204**, 412–422 (2005).
47. Bond, M., Wu, Y.-J., Sala-Newby, G. B. & Newby, A. C. Rho GTPase, Rac1, regulates Skp2 levels, vascular smooth muscle cell proliferation, and intima formation in vitro and in vivo. *Cardiovasc. Res.* **80**, 290–298 (2008).
48. Duggirala, A. *et al.* cAMP-induced actin cytoskeleton remodelling inhibits MKL1-dependent expression of the chemotactic and pro-proliferative factor, CCN1. *J. Mol. Cell. Cardiol.* **79**, 157–168 (2015).

49. Vallano, M. L., Goldenring, J. R., Buckholz, T. M., Larson, R. E. & DeLorenzo, R. J. Separation of endogenous calmodulin- and cAMP-dependent kinases from microtubule preparations. *Proc. Natl. Acad. Sci. U. S. A.* **82**, 3202–3206 (1985).

50. Dosemeci, A. & Pant, H. C. Association of cyclic-AMP-dependent protein kinase with neurofilaments. *Biochem. J.* **282 (Pt 2)**, 477–481 (1992).

51. Bamshad, M., Van Heest, A. E. & Pleasure, D. Arthrogryposis: A Review and Update. *J. Bone Jt. Surg.* **91**, 40–46 (2009).

52. Sadana, R. & Dessauer, C. W. Physiological roles for G protein-regulated adenylyl cyclase isoforms: insights from knockout and overexpression studies. *Neurosignals* **17**, 5–22 (2009).

53. Agolini, E. *et al.* Expanding the clinical and molecular spectrum of lethal congenital contracture syndrome 8 associated with biallelic variants *of ADCY6*. *Clin. Genet.* **97**, 649–654 (2020).

54. Yimenicioğlu S, Kocaağa A, & Paksoy B. Case report the novel homozygousADCY6 c. 413G>A; p. R138H gene variant associated with lethal congenitalcontracture syndrome 8 in a female patient with epilepsy and pachygyria. *HongKong J Paediatr* (2023).

55. Devasani, K. & Yao, Y. Expression and functions of adenylyl cyclases in the CNS. *Fluids Barriers CNS* **19**, 23 (2022).

56. Wang, Z., Phan, T. & Storm, D. R. The type 3 adenylyl cyclase is required for novel object learning and extinction of contextual memory: role of cAMP signaling in primary cilia. *J. Neurosci. Off. J. Soc. Neurosci.* **31**, 5557–5561 (2011).

57. Chen, X. *et al.* Ablation of Type III Adenylyl Cyclase in Mice Causes Reduced Neuronal Activity, Altered Sleep Pattern, and Depression-like Phenotypes. *Biol. Psychiatry* **80**, 836–848 (2016).

58. Iwamoto, T. *et al.* Motor Dysfunction in Type 5 Adenylyl Cyclase-null Mice. *J. Biol. Chem.* **278**, 16936–16940 (2003).

59. Gilmour, D. T., Maischein, H.-M. & Nüsslein-Volhard, C. Migration and Function of a Glial Subtype in the Vertebrate Peripheral Nervous System. *Neuron* **34**, 577–588 (2002).

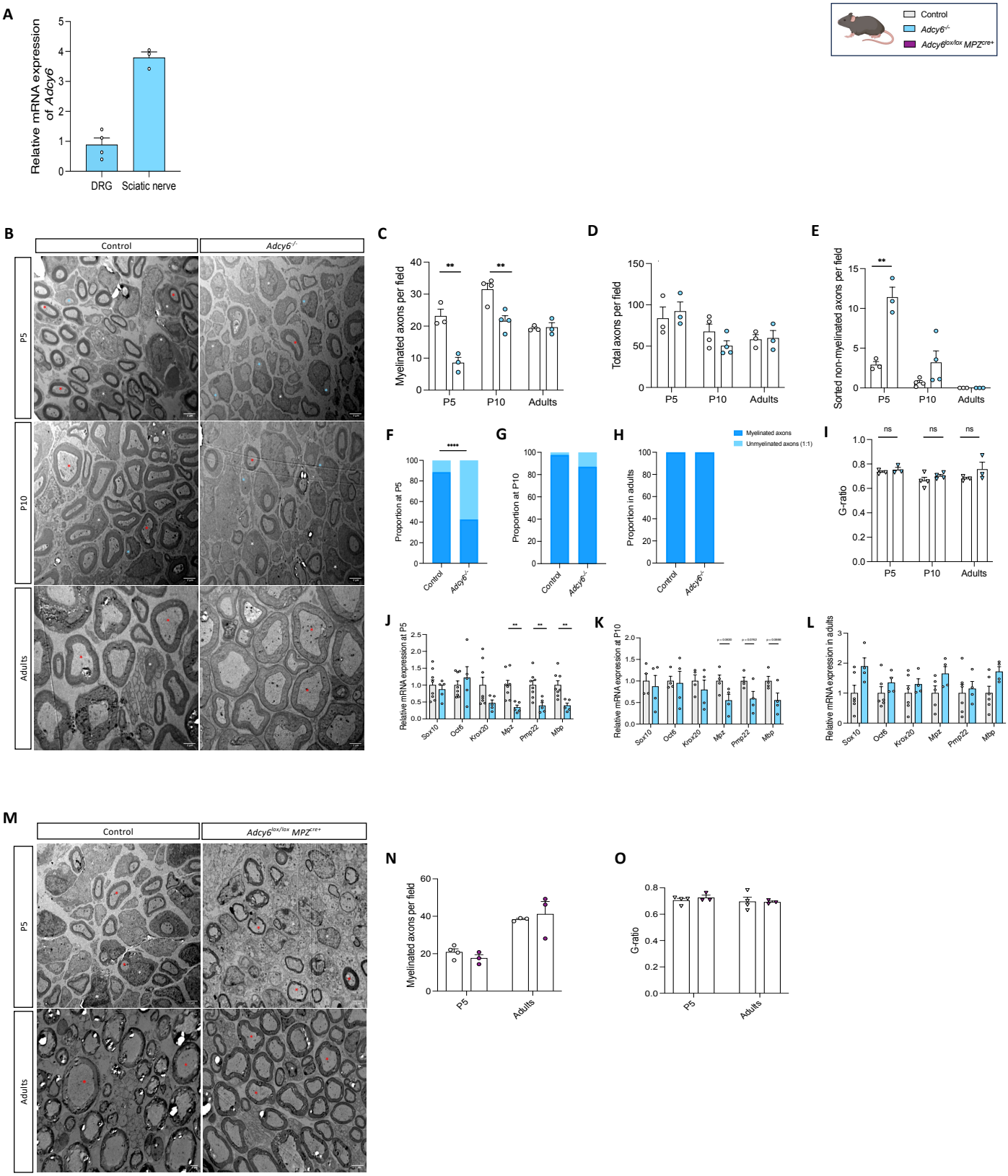

A
Relative mRNA expression of Adcy6
DRG
Sciatic nerve
Control
Adcy6-/-
Adcy6lox/lox MPZcre+
B
Control
Adcy6-/-
P5
P10
Adults
C
Myelinated axons per field
D
Total axons per field
E
Sorted non-myelinated axons per field
F
Proportion at P5
G
Proportion at P10
H
Proportion in adults
Myelinated axons
Unmyelinated axons (1:1)
I
G-ratio
ns
J
Relative mRNA expression at P5
Sox10
Oct6
Krox20
Mpz
Pmp22
Mbp
K
Relative mRNA expression at P10
L
Relative mRNA expression in adults
M
Control
Adcy6lox/lox MPZcre+
N
Myelinated axons per field
O
G-ratio

Figure 1

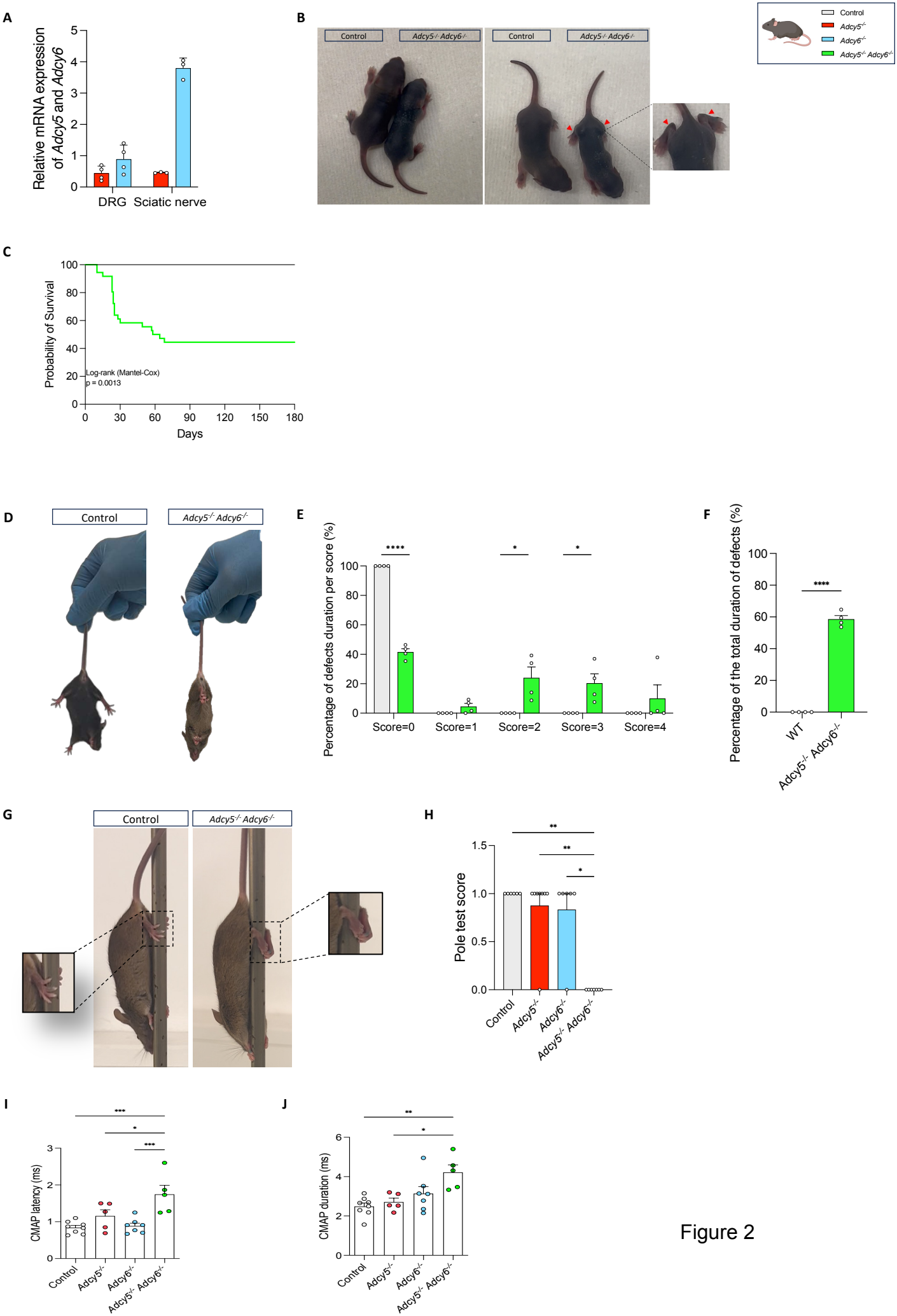

A
Relative mRNA expression of Adcy5 and Adcy6
DRG
Sciatic nerve
B
Control
Adcy5-/- Adcy6-/-
Control
Adcy5-/- Adcy6-/-
Control
Adcy5-/-
Adcy6-/-
Adcy5-/- Adcy6-/-
C
Probability of Survival
Log-rank (Mantel-Cox)
p = 0.0013
Days
D
Control
Adcy5-/- Adcy6-/-
E
Percentage of defects duration per score (%)
Score=0
Score=1
Score=2
Score=3
Score=4
F
Percentage of the total duration of defects (%)
WT
Adcy5-/- Adcy6-/-
G
Control
Adcy5-/- Adcy6-/-
H
Pole test score
Control
Adcy5-/-
Adcy6-/-
Adcy5-/- Adcy6-/-
I
CMAP latency (ms)
Control
Adcy5-/-
Adcy6-/-
Adcy5-/- Adcy6-/-
J
CMAP duration (ms)
Control
Adcy5-/-
Adcy6-/-
Adcy5-/- Adcy6-/-

Figure 2

Figure 3

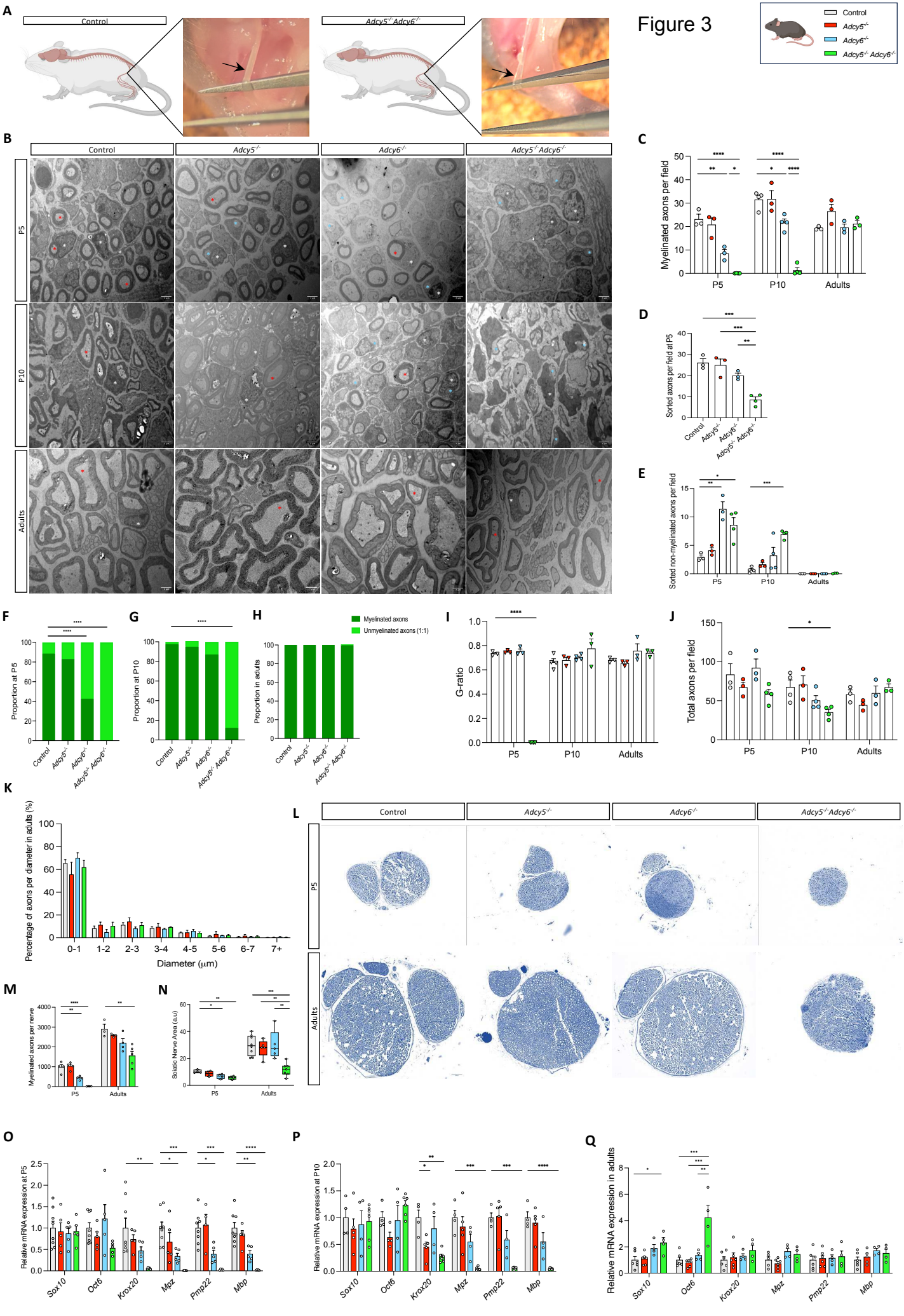
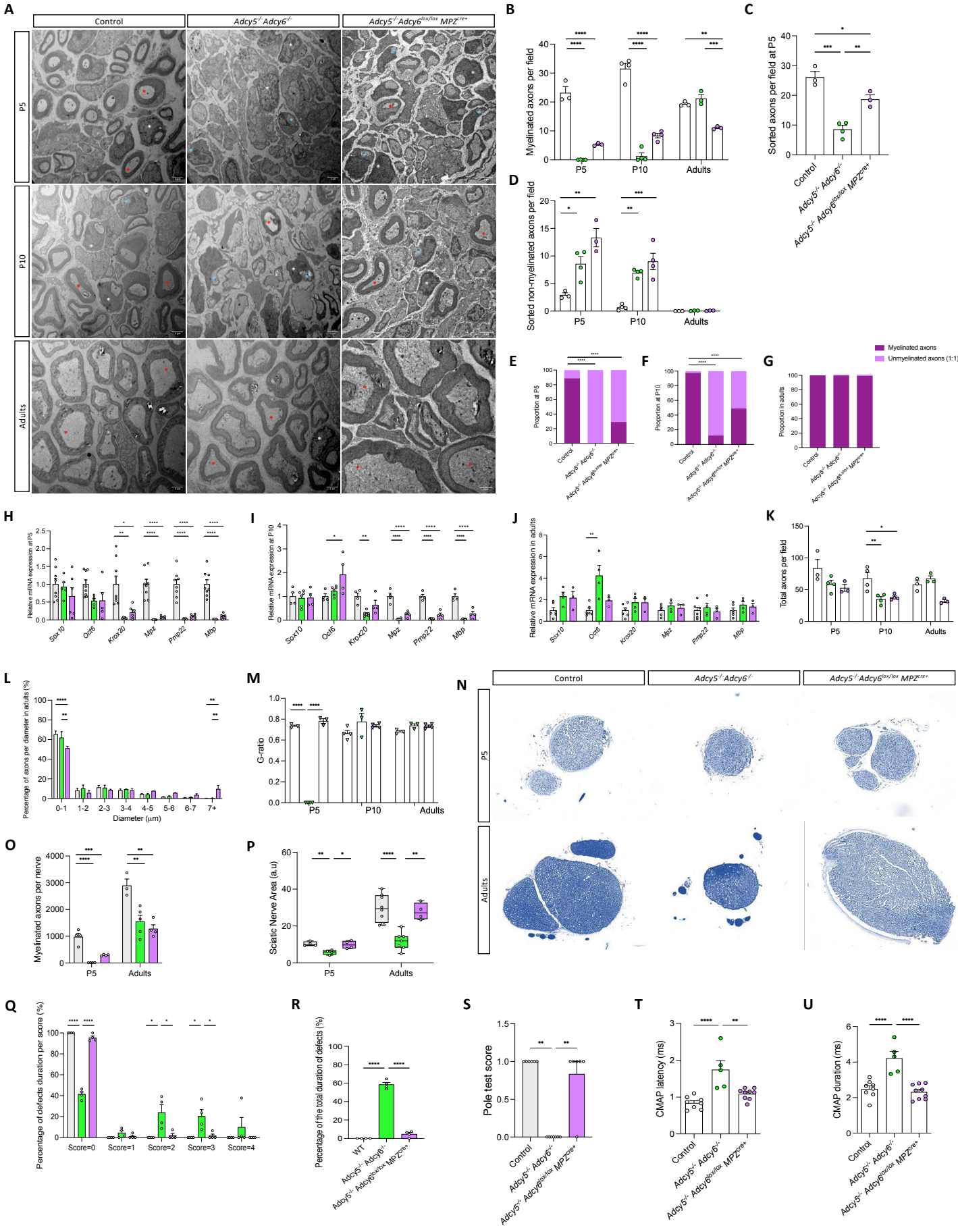

A
Control
Adcy5-/- Adcy6-/-
Control
Adcy5-/-
Adcy6-/-
Adcy5-/- Adcy6-/-
B
Control
Adcy5-/-
Adcy6-/-
Adcy5-/- Adcy6-/-
P5
P10
Adults
C
Myelinated axons per field
P5
P10
Adults
D
Sorted axons per field at P5
E
Sorted non-myelinated axons per field
F
Proportion at P5
G
Proportion at P10
H
Proportion in adults
Myelinated axons
Unmyelinated axons (1:1)
I
G-ratio
J
Total axons per field
K
Percentage of axons per diameter in adults (%)
0-1
1-2
2-3
3-4
4-5
5-6
6-7
7+
Diameter (µm)
L
M
Myelinated axons per nerve
N
Sciatic Nerve Area (a.u)
O
Relative mRNA expression at P5
Sox10
Oct6
Krox20
Mpz
Pmp22
Mbp
P
Relative mRNA expression at P10
Q
Relative mRNA expression in adults

Figure 4


Control
Adcy5-/- Adcy6-/-
Adcy5-/- Adcy6lox/lox MPZcre+
A
B
C
D
E
F
G
H
I
J
K
L
M
N
O
P
Q
R
S
T
U
P5
P10
Adults
Myelinated axons per field
Sorted axons per field at P5
Sorted non-myelinated axons per field
Myelinated axons
Unmyelinated axons (1:1)
Proportion at P5
Proportion at P10
Proportion in adults
Relative mRNA expression at P5
Relative mRNA expression at P10
Relative mRNA expression in adults
Total axons per field
Sox10
Oct6
Krox20
Mpz
Pmp22
Mbp
Percentage of axons per diameter in adults (%)
Diameter (µm)
G-ratio
Myelinated axons per nerve
Sciatic Nerve Area (a.u)
Percentage of defects duration per score (%)
Score=0
Score=1
Score=2
Score=3
Score=4
Percentage of the total duration of defects (%)
WT
Pole test score
CMAP latency (ms)
CMAP duration (ms)

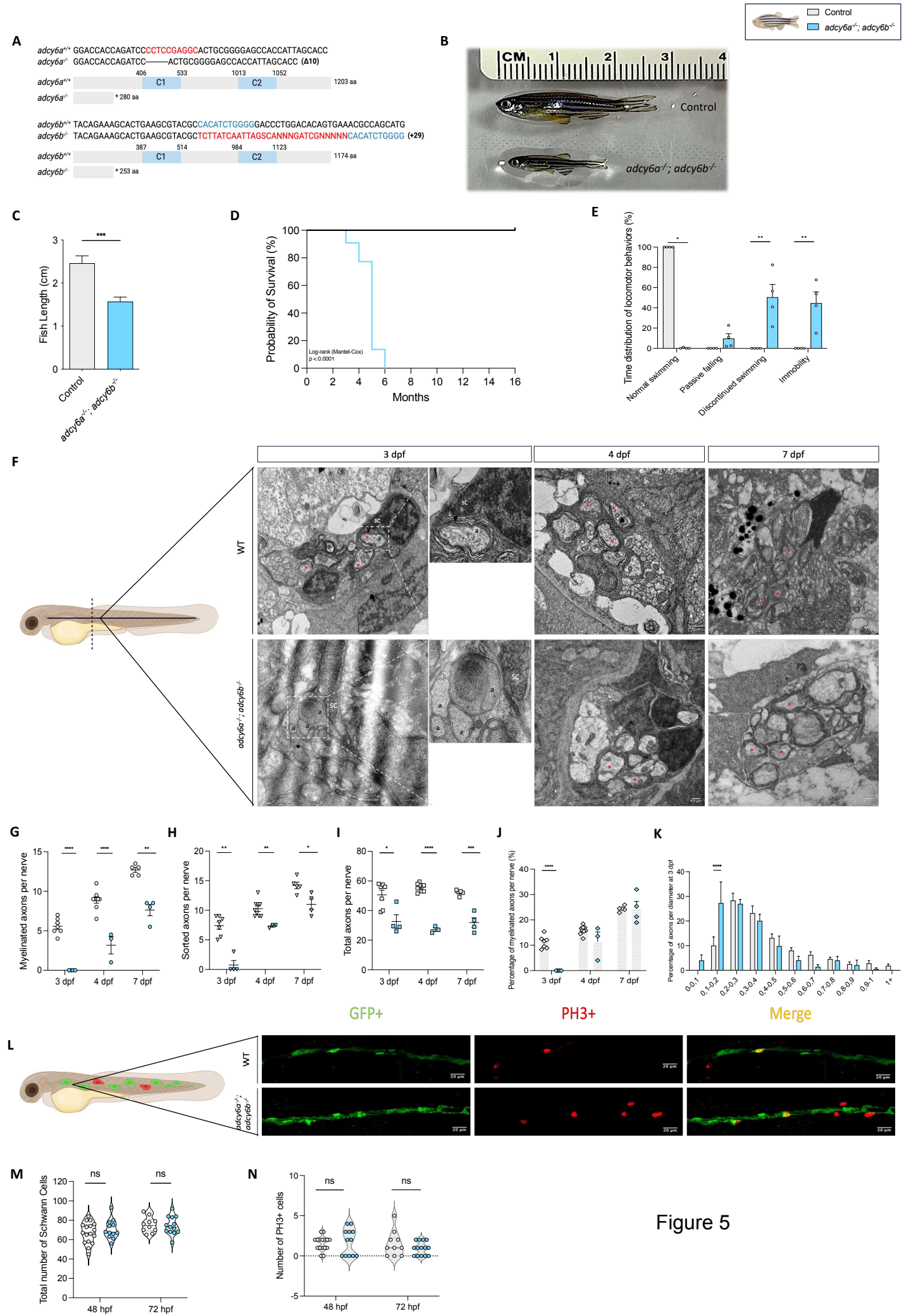

A
adcy6a+/+ GGACCACCAGATCCCCTCCGAGGCACTGCGGGGAGCCACCATTAGCACC
adcy6a-/- GGACCACCAGATCC--------ACTGCGGGGAGCCACCATTAGCACC (Δ10)
406
533
1013
1052
C1
C2
1203 aa
* 280 aa
adcy6b+/+ TACAGAAAGCACTGAAGCGTACGCCACATCTGGGGGACCCTGGACACAGTGAAACGCCAGCATG
adcy6b-/- TACAGAAAGCACTGAAGCGTACGCTCTTATCAATTAGSCANNNGATCGNNNNNCACATCTGGGG (+29)
387
514
984
1123
1174 aa
* 253 aa
B
CM
Control
adcy6a-/-; adcy6b-/-
C
Fish Length (cm)
***
Control
adcy6a-/-; adcy6b-/-
D
Probability of Survival (%)
Log-rank (Mantel-Cox)
p<0.0001
Months
E
Time distribution of locomotor behaviors (%)
Normal swimming
Passive falling
Discontinued swimming
Immobility
F
3 dpf
4 dpf
7 dpf
WT
adcy6a-/-; adcy6b-/-
SC
a
G
Myelinated axons per nerve
H
Sorted axons per nerve
I
Total axons per nerve
J
Percentage of myelinated axons per nerve (%)
K
Percentage of axons per diameter at 3 dpf
0-0.1
0.1-0.2
0.2-0.3
0.3-0.4
0.4-0.5
0.5-0.6
0.6-0.7
0.7-0.8
0.8-0.9
0.9-1
1+
GFP+
PH3+
Merge
L
WT
adcy6a-/-; adcy6b-/-
20 µm
M
Total number of Schwann Cells
ns
48 hpf
72 hpf
N
Number of PH3+ cells
ns
48 hpf
72 hpf

Figure 5

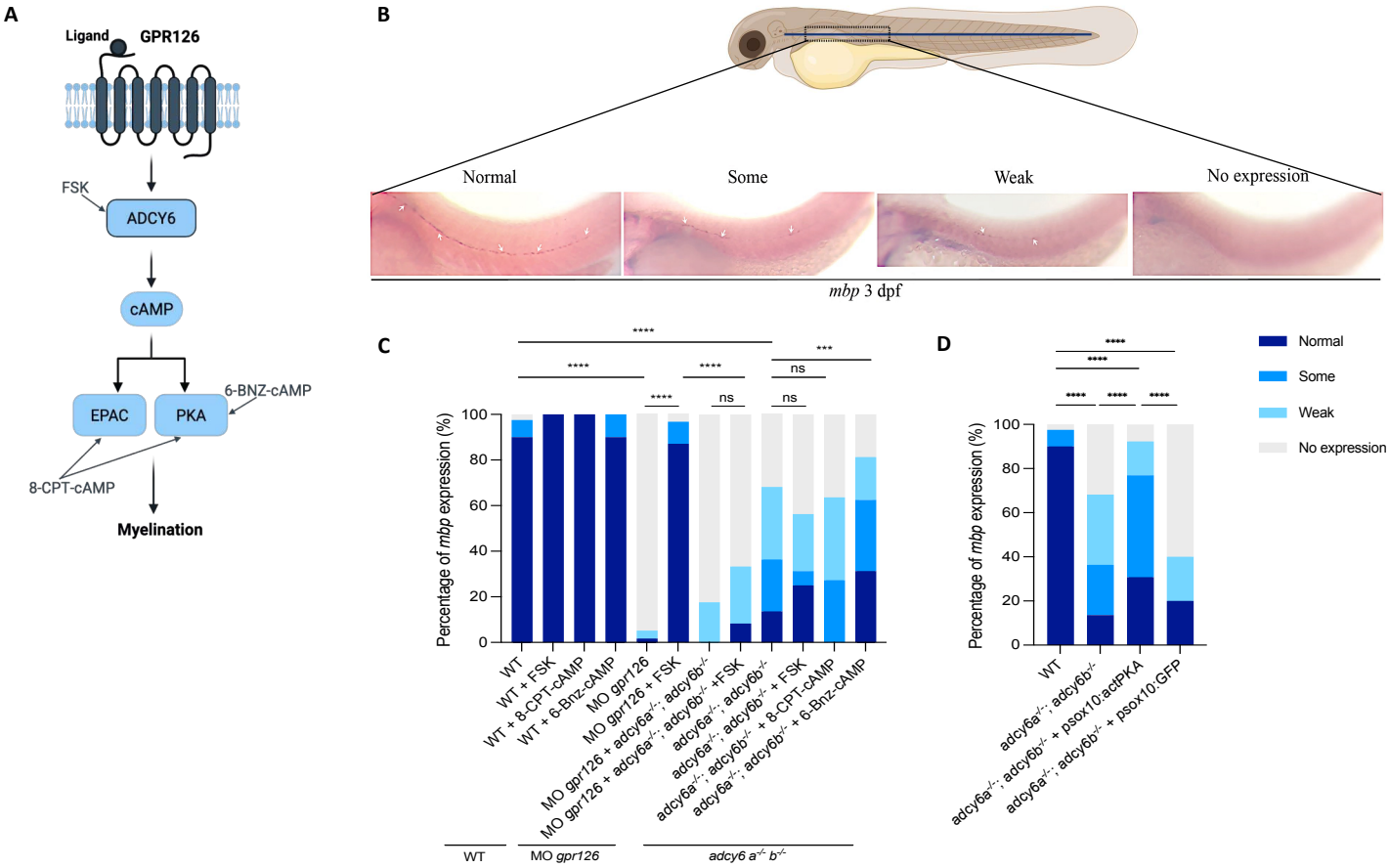

A
Ligand
GPR126
FSK
ADCY6
cAMP
EPAC
PKA
6-BNZ-cAMP
8-CPT-cAMP
Myelination
B
Normal
Some
Weak
No expression
mbp 3 dpf
C
Percentage of mbp expression (%)
WT
WT + FSK
WT + 8-CPT-cAMP
WT + 6-Bnz-cAMP
MO gpr126
MO gpr126 + FSK
MO gpr126 + adcy6a-/-; adcy6b-/-
MO gpr126 + adcy6a-/-; adcy6b-/- +FSK
adcy6a-/-; adcy6b-/-
adcy6a-/-; adcy6b-/- + FSK
adcy6a-/-; adcy6b-/- + 8-CPT-cAMP
adcy6a-/-; adcy6b-/- + 6-Bnz-cAMP
WT
MO gpr126
adcy6 a-/- b-/-
D
Percentage of mbp expression (%)
WT
adcy6a-/-; adcy6b-/-
adcy6a-/-; adcy6b-/- + psox10:actPKA
adcy6a-/-; adcy6b-/- + psox10:GFP
Normal
Some
Weak
No expression

Figure 6

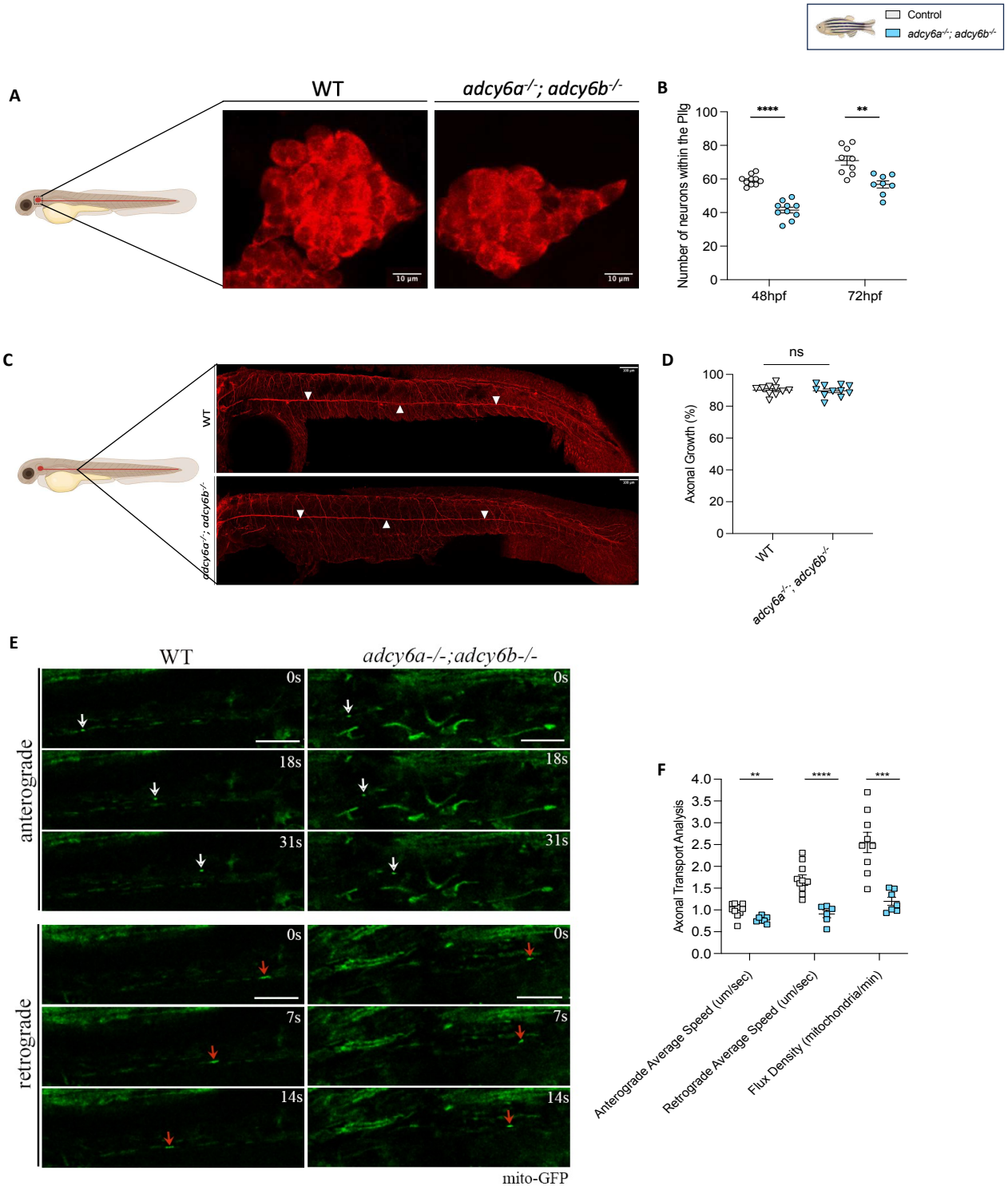

Control
adcy6a-/-; adcy6b-/-
A
WT
adcy6a-/-; adcy6b-/-
10 µm
10 µm
B
Number of neurons within the Pllg
****
**
48hpf
72hpf
C
WT
adcy6a-/-; adcy6b-/-
D
ns
Axonal Growth (%)
WT
adcy6a-/-; adcy6b-/-
E
WT
adcy6a-/-;adcy6b-/-
anterograde
retrograde
0s
18s
31s
7s
14s
mito-GFP
F
Axonal Transport Analysis
**
****
***
Anterograde Average Speed (um/sec)
Retrograde Average Speed (um/sec)
Flux Density (mitochondria/min)

Figure 7

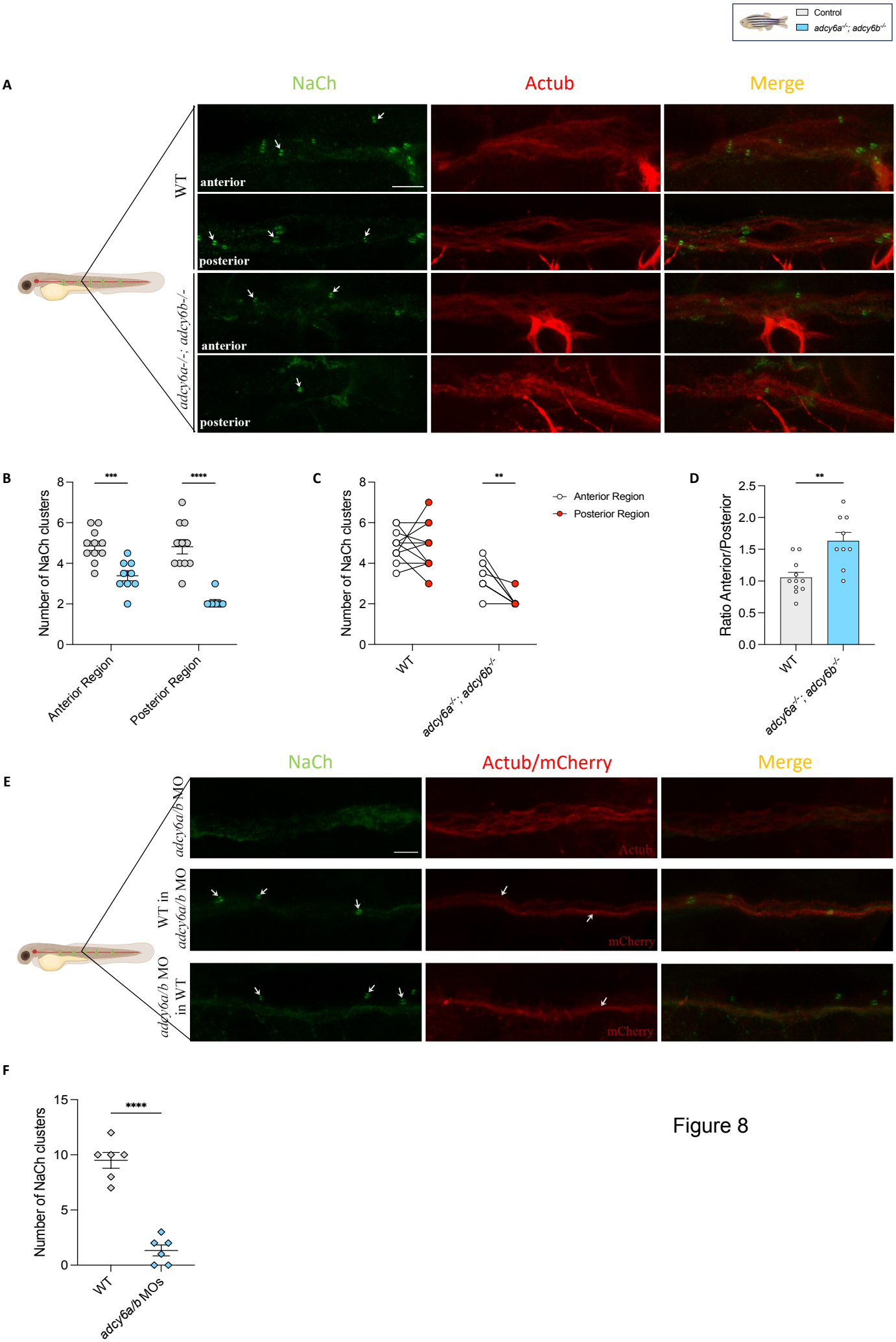

Control
adcy6a-/-; adcy6b-/-
A
NaCh
Actub
Merge
WT
anterior
posterior
adcy6a-/-; adcy6b-/-
anterior
posterior
B
Number of NaCh clusters
***
****
Anterior Region
Posterior Region
C
Number of NaCh clusters
**
Anterior Region
Posterior Region
WT
adcy6a-/-; adcy6b-/-
D
Ratio Anterior/Posterior
**
WT
adcy6a-/-; adcy6b-/-
E
NaCh
Actub/mCherry
Merge
adcy6a/b MO
Actub
WT in adcy6a/b MO
mCherry
adcy6a/b MO in WT
mCherry
F
Number of NaCh clusters
****
WT
adcy6a/b MOs

Figure 8

Supplementary Files

This is a list of supplementary files associated with this preprint. Click to download.

- FigureS1.pdf
- FigureS2.pdf
- FigureS3.pdf
- FigureS4.pdf
- FigureS5.pdf
- FigureS6.pdf
- MovieS1.mov
- MovieS2.mov
- MovieS3.mov
- MovieS4.mp4
- MovieS5.avi
- MovieS6.avi
- MovieS7.avi
- MovieS8.avi
- MovieS9.avi
- Supplementaryinformation.pdf